AUTOPHAGY
2019, VOL. 15, NO. 1, 131–150
https://doi.org/10.1080/15548627.2018.1511263

Taylor & Francis
Taylor & Francis Group

RESEARCH PAPER - BASIC SCIENCE

Thyroid hormone (T_3) stimulates brown adipose tissue activation via mitochondrial biogenesis and MTOR-mediated mitophagy

Winifred W. Yau[a], Brijesh K. Singh[a], Ronny Lesmana[a,b,c], Jin Zhou[a], Rohit A. Sinha[a,d], Kiraely A. Wong[a], Yajun Wu[e], Boon-Huat Bay[e], Shigeki Sugii[a,f], Lei Sun[a], and Paul M. Yen[a,g]

[a]Laboratory of Hormonal Regulation, Cardiovascular and Metabolic Disorders Program, Duke-NUS Medical School, Singapore; [b]Physiology Division, Department of Anatomy, Physiology and Biology Cell, Faculty of Medicine, Universitas Padjadjaran, Bandung, Indonesia; [c]Central laboratory, Universitas Padjadjaran, Bandung, Indonesia; [d]Department of Endocrinology, Sanjay Gandhi Postgraduate Institute of Medical Sciences, Lucknow, India; [e]Department of Anatomy, Yong Loo Lin School of Medicine, National University of Singapore, Singapore; [f]Fat Metabolism and Stem Cell Group, Singapore Bioimaging Consortium, A*STAR, Singapore; [g]Sarah W. Stedman Nutrition and Metabolism Center, Departments of Medicine and Pharmacology and Cancer Biology, Duke University Medical Center, Durham, NC, USA

ABSTRACT

The thyroid hormone triiodothyronine (T_3) activates thermogenesis by uncoupling electron transport from ATP synthesis in brown adipose tissue (BAT) mitochondria. Although T_3 can induce thermogenesis by sympathetic innervation, little is known about its cell autonomous effects on BAT mitochondria. We thus examined effects of T_3 on mitochondrial activity, autophagy, and metabolism in primary brown adipocytes and BAT and found that T_3 increased fatty acid oxidation and mitochondrial respiration as well as autophagic flux, mitophagy, and mitochondrial biogenesis. Interestingly, there was no significant induction of intracellular reactive oxygen species (ROS) despite high mitochondrial respiration and UCP1 induction by T_3. However, when cells were treated with *Atg5* siRNA to block autophagy, induction of mitochondrial respiration by T_3 decreased, and was accompanied by ROS accumulation, demonstrating a critical role for autophagic mitochondrial turnover. We next generated an *Atg5* conditional knockout mouse model (*Atg5* cKO) by injecting *Ucp1* promoter-driven *Cre*-expressing adenovirus into $Atg5^{Flox/Flox}$ mice to examine effects of BAT-specific autophagy on thermogenesis *in vivo*. Hyperthyroid *Atg5* cKO mice exhibited lower body temperature than hyperthyroid or euthyroid control mice. Metabolomic analysis showed that T_3 increased short and long chain acylcarnitines in BAT, consistent with increased β-oxidation. T_3 also decreased amino acid levels, and in conjunction with SIRT1 activation, decreased MTOR activity to stimulate autophagy. In summary, T_3 has direct effects on mitochondrial autophagy, activity, and turnover in BAT that are essential for thermogenesis. Stimulation of BAT activity by thyroid hormone or its analogs may represent a potential therapeutic strategy for obesity and metabolic diseases.

Abbreviations: ACACA: acetyl-Coenzyme A carboxylase alpha; AMPK: AMP-activated protein kinase; *Acsl1*: acyl-CoA synthetase long-chain family member 1; ATG5: autophagy related 5; ATG7: autophagy related 7; ATP: adenosine triphosphate; BAT: brown adipose tissue; cKO: conditional knockout; COX4I1: cytochrome c oxidase subunit 4I1; *Cpt1b*: carnitine palmitoyltransferase 1b, muscle; CQ: chloroquine; DAPI: 4′,6-diamidino-2-phenylindole; DIO2: deiodinase, iodothyronine, type 2; DMEM: Dulbecco's modified Eagle's medium; EIF4EBP1: eukaryotic translation initiation factor 4E binding protein 1; *Fabp4*: fatty acid binding protein 4, adipocyte; FBS: fetal bovine serum; FCCP: carbonyl cyanide-4-(trifluoromethoxy) phenylhydrazone; FGF: fibroblast growth factor; FOXO1: forkhead box O1; GAPDH: glyceraldehyde-3-phosphate dehydrogenase; GFP: green fluorescent protein; *Gpx1*: glutathione peroxidase 1; *Lipe*: lipase, hormone sensitive; MAP1LC3B: microtubule-associated protein 1 light chain 3; mRNA: messenger RNA; MTORC1: mechanistic target of rapamycin kinase complex 1; NAD: nicotinamide adenine dinucleotide; *Nrf1*: nuclear respiratory factor 1; OCR: oxygen consumption rate; PBS: phosphate-buffered saline; PCR: polymerase chain reaction; PPARGC1A: peroxisome proliferative activated receptor, gamma, coactivator 1 alpha; *Pnpla2*: patatin-like phospholipase domain containing 2; *Prdm16*: PR domain containing 16; PRKA: protein kinase, AMP-activated; RPS6KB: ribosomal protein S6 kinase; RFP: red fluorescent protein; ROS: reactive oxygen species; SD: standard deviation; SEM: standard error of the mean; siRNA: small interfering RNA; SIRT1: sirtuin 1; *Sod1*: superoxide dismutase 1, soluble; *Sod2*: superoxide dismutase 2, mitochondrial; SQSTM1: sequestosome 1; T_3: 3,5,3′-triiodothyronine; TFEB: transcription factor EB; TOMM20: translocase of outer mitochondrial membrane 20; UCP1: uncoupling protein 1 (mitochondrial, proton carrier); ULK1: unc-51 like kinase 1; VDAC1: voltage-dependent anion channel 1; WAT: white adipose tissue

ARTICLE HISTORY
Received 12 June 2017
Revised 26 July 2018
Accepted 8 August 2018

KEYWORDS
Autophagy; brown adipose tissue; mitochondria; mitophagy; thermogenesis; thyroid hormone

CONTACT Paul M. Yen paul.yen@duke-nus.edu.sg Laboratory of Hormonal Regulation, Cardiovascular and Metabolic Disorders Program, Duke-NUS Medical School, 8 College Road, 169857, Singapore

Supplementary data for this article can be accessed here.

Introduction

The 2 forms of thyroid hormones, thyroxine (T_4) and its active metabolite 3,5,3′-triiodothyronine (T_3), regulate metabolic processes that control energy utilization. The intracellular levels of these hormones are controlled by DIO1 (deiodinase, iodothyronine, type 1) and DIO2 that catalyze the conversion of T_4 to its active form T_3 [1]. In homeothermic species, these processes are important in generating heat to maintain body temperature. T_3 has long been implicated in stimulating both obligatory and adaptive thermogenesis in various tissues [2–4]. Especially in brown adipose tissue (BAT), T_3 stimulates thermogenesis by inducing metabolic inefficiency through the induction of the mitochondrial uncoupling protein, UCP1 [2,3]. The opposite occurs in the absence of T_3, as thermogenic capacity of brown adipose tissue (BAT) is greatly reduced [5]. Clinically, these effects are manifested by hyperthermia and hypothermia observed in patients with severe hyperthyroidism and hypothyroidism, respectively.

BAT is present in almost all eutherian mammals and is responsible for non-shivering adaptive thermogenesis [6]. It is prominent in neonates and small mammals, and also metabolically active in adult humans, especially in response to cold. Due to its ability to oxidize fatty acids and increase glucose utilization by lowering insulin resistance, pharmacological activation of BAT has been considered an attractive potential therapeutic approach to treat obesity and diabetes [7]. Fetal rat BAT has DIO2 expression, suggesting that T_3 may be responsible for embryonic development of BAT [8]. In addition, mouse embryos with targeted disruption of DIO2 show impaired adipogenesis (decreased expression of *Fabp4*/*aP2, Cidea*, and *Acsl5*) and adaptive thermogenesis (decreased expression of *Ucp1* and *Ppargc1a*) [9]. These defects persist throughout adulthood as adaptive thermogenesis is hindered by loss of T_3-mediated lipogenesis and lipolysis [5,10]. Thyroid status also is highly correlated with BAT activity in mice. Hyperthyroid mice have higher BAT volume, fatty acid oxidation, and glucose uptake [11]. In mature BAT, there is increased adaptive thermogenesis by the sympathetic nervous system (SNS) in response to cold. T_3 also increases hypothalamic stimulation of sympathetic nervous system to induce DIO2 expression and increase local conversion from T_4 to T_3 to increase UCP1 expression [4,5,12–15]. Additionally, catecholamines increase the intracellular cAMP level, protein kinase A activity and hormone-sensitive lipase (LIPE/HSL) phosphorylation to stimulate lipolysis in both WAT and BAT to provide fatty acid substrates for β-oxidation [16]. T_3 increases adrenergic stimulation of UCP1 expression *in vivo* [17–20] and may sensitize cultured brown adipocytes to adrenergic stimulation of UCP1 expression [21]. On the other hand, T_3 has been reported to induce UCP1 expression in fetal rat brown adipocytes in primary culture without any adrenergic stimulation [22]. Thus, the question of a cell autonomous role of T_3 on BAT currently is unresolved.

In metabolically active tissues, autophagy is necessary for efficient turnover of damaged organelles such as mitochondria (mitophagy). Mice with an adipose-specific deletion of *Atg7* (autophagy related 7) have more mitochondria in adipose tissues [23] suggesting that autophagy is essential for mitochondrial clearance. Recently, Martinez-Lopez et al. and Mottillo et al. have found that cold exposure at 4°C induces lipophagy and mitophagy in BAT [24,25], suggesting that autophagy is needed for adaptive thermogenesis. We have recently shown that T_3 maintains mitochondrial homeostasis by inducing autophagy of lipids (lipophagy) and mitophagy in liver and skeletal muscle [26,27]. We thus investigated whether T_3 has a cell autonomous role on the activation of BAT by examining autophagy, mitochondrial turnover, fatty acid metabolism, and mitochondrial respiration in primary brown adipocytes and a brown adipocyte cell line in cell culture studies as well as performing *in vivo* experiments in both hyperthyroid and BAT-specific *Atg5* conditional knockout mouse models at room temperature in order to minimize the contribution from sympathetic stimulation. Our findings showed that T_3 has cell autonomous effects on mitochondrial activity, biogenesis, mitophagy, and lipid metabolism in BAT, and suggest that T_3 or its analogs may have potential beneficial effects on obesity by directly stimulating BAT activity.

Results

T_3 induces autophagic flux in BAT, primary brown adipocytes, and mBAP9 cells

To investigate the effect of T_3 on autophagy in BAT, we examined BAT samples from hyperthyroid mice that were treated with T_3 (10 μg/100 g body weight) for 10 d at room temperature. We found increased lipidated MAP1LC3B/LC3B (MAP1LC3B-II) and reduced SQSTM1/p62 levels in BAT from hyperthyroid mice, indicating that there was increased autophagic flux (Figure 1(a)). Accordingly, we observed more autophagic vesicles in electron microscopy images of hyperthyroid BAT (Figures 1(b) and S1(a)). In primary brown adipocytes, T_3 also increased the MAP1LC3B-II level in a time- and dose-dependent manner (Figures 1(c) and S1 (b)) without affecting cell viability (Figure S1(c)), and was consistent with increased number of autophagic vesicles in T_3-treated primary brown adipocytes (Figures 1(d) and S1 (d)). Bafilomycin A_1 (Baf), a pharmacological inhibitor of vacuolar H^+ ATPase/lysosomal acidification, caused MAP1LC3B-II accumulation in BAT; however, when it was added together with T_3, there was a further increase in MAP1LC3B-II level compared to samples treated with T_3 alone, strongly suggesting that T_3 stimulated synthesis of new autophagosomes and increased autophagic flux (Figure 1(e)). We further demonstrated autophagic flux by transfecting a tandem fluorescent MAP1LC3B (RFP-eGFP-MAP1LC3B) plasmid expressing MAP1LC3B with the green and red fluorescent domains into a brown adipocyte mouse mBAP-9 cell line. When this fusion protein is incorporated within an autophagosome, both green and red signals are emitted, resulting in a yellow color in overlay image. However, when the autophagosome fuses with a lysosome to form an autolysosome, the acidic environment quenches the green signal and only red signal is detected. Therefore, the

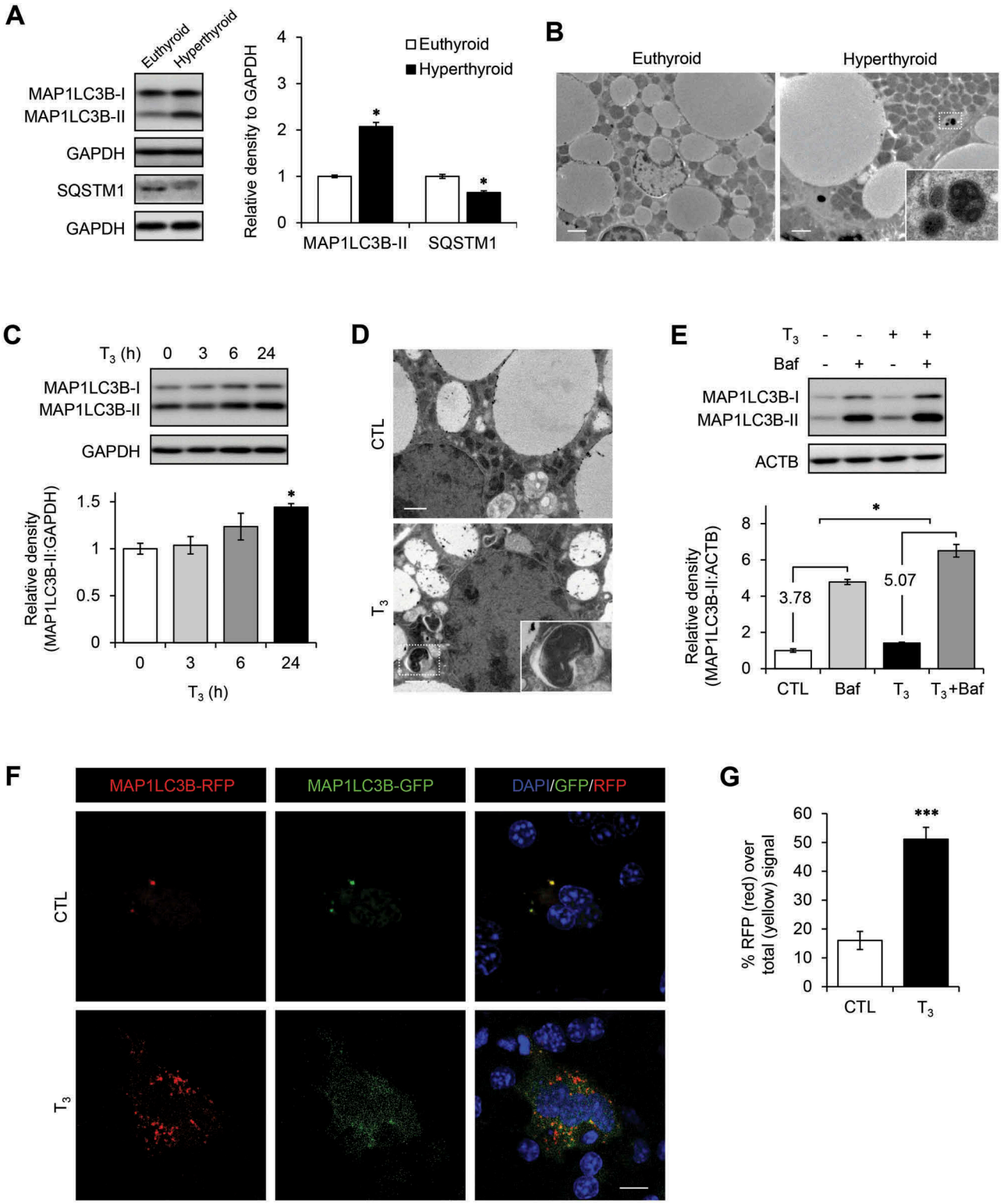

Figure 1. T_3 induces autophagy in BAT and brown adipocytes. (a) Increased autophagic flux in T_3-treated BATs. Immunoblots and densitometry showing MAP1LC3B-II and SQSTM1 levels in BATs of hyperthyroid mice. Results represent mean ± SEM (n = 3). (b) Electron microscopy images showing increased number of autophagic vesicles in hyperthyroid BAT. Scale bar: 2 µm. (c) Time course of MAP1LC3B-II induction in primary brown adipocytes treated with 10 nM T_3 for 0, 3, 6 and 24 h. (d) Electron microscopy images showing increased number of autophagic vesicles in primary brown adipocytes treated with 10 nM T_3 for 24 h. Scale bar: 1 µm. (e) Autophagic flux analysis showing accumulation of MAP1LC3B-II following autophagy inhibition. Primary brown adipocytes were treated with 10 nM T_3 for 24 h. Cells were treated with 50 nM Baf to block autophagosome clearance 6 h before harvest. Result shows mean ± SD (n = 3) where n represents number of independent experiments. (f) Confocal images showing brown adipocyte cell line mBAP-9 transfected with eGFP-MAP1LC3B plasmid and treated with 10 nM T_3 for 24 h. Yellow color represents MAP1LC3B-II on autophgosomes. Red color represents MAP1LC3B-II on lysosomes. Scale bar: 10 µm. (g) Quantitative analysis of the RFP (red) fluorescence relative to total (yellow) signal. Quantification of images (at least 10 transfected cells per each sample in 3 different fields) was done using ImageJ software. Result shows mean ± SD. *: $P < 0.05$, **: $P < 0.01$, ***: $P < 0.001$.

amount of red signal reflects the rate of autophagic flux. Confocal images of T_3-treated brown adipocytes showed increases in the number of red puncta (Figure 1(f)) and the red to yellow signal ratios (Figure 1(g)), indicating that they had higher autophagic flux than control brown adipocytes.

T3 increases mitophagy in BAT, primary brown adipocytes, and mBAP-9 cells

To investigate mitophagy *in vivo*, we used the lysosomal inhibitor, chloroquine (CQ), to block autophagy clearance in hyperthyroid mice. We found increased accumulation of the mitochondrial proteins, COX4I1 (cytochrome c oxidase subunit 4I1) and TOMM20 (translocase of outer mitochondrial membrane 20), in BAT from hyperthyroid mice (Figures 2(a) and S2(a)), suggesting that mitochondrial clearance was dependent on autophagy (mitophagy). Mitochondrial remnants also were observed inside autophagic vesicles in electron microscopic images from CQ-treated hyperthyroid mice (Figure 2(b)) and in primary brown adipocytes treated with Baf and T_3 (data not shown). Baf increased accumulation of TOMM20 (a mitochondrial outer membrane protein) and VDAC1 (voltage-dependent anion channel 1; a major isoform highly and predominantly expressed on the mitochondrial outer membrane) (basal mitophagy) in primary brown adipocytes; however, when both Baf and T_3 were given together, there was a further increase in accumulation of TOMM20 and VDAC1 in primary brown adipocytes (Figure 2(c)). These *in vivo* and cell culture studies strongly suggested that mitochondria were *bona fide* cargoes of T_3-induced autophagy. To further confirm these observations, a tandem-tagged mito-RFP-EGFP plasmid, which encodes a fusion protein containing a mitochondrial targeting signal alongside green and red fluorescent proteins, was transfected into mBAP-9 brown adipocyte cells (Figure 2(d)). At cytosolic pH levels, mitochondria fluoresce at both green and red wavelengths resulting in a yellow color. However, in the low-pH environment within autolysosomes, the green signal is quenched and only red color is emitted. T_3 treatment increased the number of red puncta (Figure 2(d)) and the amount of red to yellow signal ratio (Figure 2(e)), demonstrating that T_3 increased mitophagy. To further visualize lysosomal mitochondria, we transfected a pMT-mKeima-Red plasmid into mBAP-9 brown adipocyte cells (Figure S2(b)). The plasmid encodes a fusion protein that targets the fluorescent protein Keima to the mitochondrial matrix. Keima is a pH-sensitive fluorescent protein that has dual excitation wavelengths. At the physiological pH of the mitochondria, the protein preferentially excites at 440 nm. Under acidic environment inside autolysosomes, the excitation wavelength is shifted to 550 nm. Using this technique, we found that T_3 treatment increased the number of lysosome-resident mitochondria in primary brown adipocytes (Figure S2(c)), confirming that T_3 directly activated mitophagy. Consistent with increased mitophagy, we also detected higher levels of SQSTM1 and MAP1LC3B-II in the mitochondrial fraction of T_3-treated BAT and primary brown adipocytes (Figure S2(d,e)). Last, we observed a higher percentage of cells that had colocalization of SQSTM1 and mitochondria marker, MitoTracker Red, in T_3-treated primary brown adipocytes using immunohistochemistry and confocal microscopy (Figure S2(f,g)).

T3 induces mitochondrial biogenesis and mitochondrial turnover in BAT, primary brown adipocytes, and mBAP-9 cells

To better understand the regulation of mitochondrial homeostasis in BAT, we examined whether T_3 increased expression of genes involved in mitochondrial pathways and biogenesis in BAT. We found that expression of genes involved in thermogenesis (*Ucp1, Prdm16, Ppargc1a*), fatty acid oxidation (*Cpt1b, Acsl1*) and lipolysis (*Pnpla2, Lipe*) were induced in BAT from hyperthyroid mice (Figure 3(a)). T_3 also increased the expression of mitochondrial proteins, COX4I1, TOMM20, VDAC1, and UCP1 (Figure 3(b)), as well and mitochondrial DNA copy number (Figure 3(c)). The increase in *Ucp1* mRNA and UCP1 protein expression was similar to those observed for other mitochondrial proteins, suggesting that its induction by T_3 was likely due to an overall increase in mitochondrial biogenesis rather than distinct pattern of expression that was unrelated to other mitochondrial proteins. Additionally, T_3 increased mitochondrial thermogenic gene mRNA (Figure 3(d)), and protein (Figure 3(e)) expression in primary mature brown adipocytes.

To further investigate the dual regulation of mitochondrial biogenesis and mitophagy (mitochondrial turnover) by T_3, we employed the recently described MitoTimer methodology [28,29] in mBAP-9 cells. pMitoTimer expresses a mutant version of DsRed, a protein that fluoresces from green to red over 48 h specifically in mitochondria, and thus can help distinguish newly synthesized mitochondria from mature mitochondria. When we examined the effects of T_3 on mitochondrial turnover, there was decreased red signal and increased green signal after 6 and 24 h of T_3 treatment (Figure 3(f)). These findings showed that T_3 simultaneously increased both mitochondrial synthesis and clearance, however, since overall levels of mitochondrial proteins were higher after T_3 treatment (Figure 3(b,e)), new mitochondrial synthesis predominated over clearance.

T3 increases fatty acid oxidation in BAT and increases mitochondrial respiration in primary brown adipocytes

Since T_3 induces both mitophagy and mitochondrial biogenesis, we further investigated whether T_3 stimulates overall mitochondrial activity. Acyl-CoAs are translocated as acylcarnitines into the mitochondrial matrix where they undergo fatty acid β-oxidation. Using a metabolomics approach, we found that the levels of short chain acylcarnitine, C2 (acetyl-carnitines), C3 (propionyl-carnitines), C4 (butyryl-carnitines) and long chain acylcarnitines were higher in BAT from hyperthyroid mice (Figure 4(a,b)), in conjunction with increased *Cpt1b* mRNA (Figure 3(a)). The increase in C2 and C4 levels suggested that there was increased acylcarnitine flux due to fatty acid β-oxidation since they are the end products of fatty acid β-oxidation (Figure 4(a)). The elevated C3 level suggested that there was increased oxidation of isoleucine, valine, threonine, and methionine since C3 is

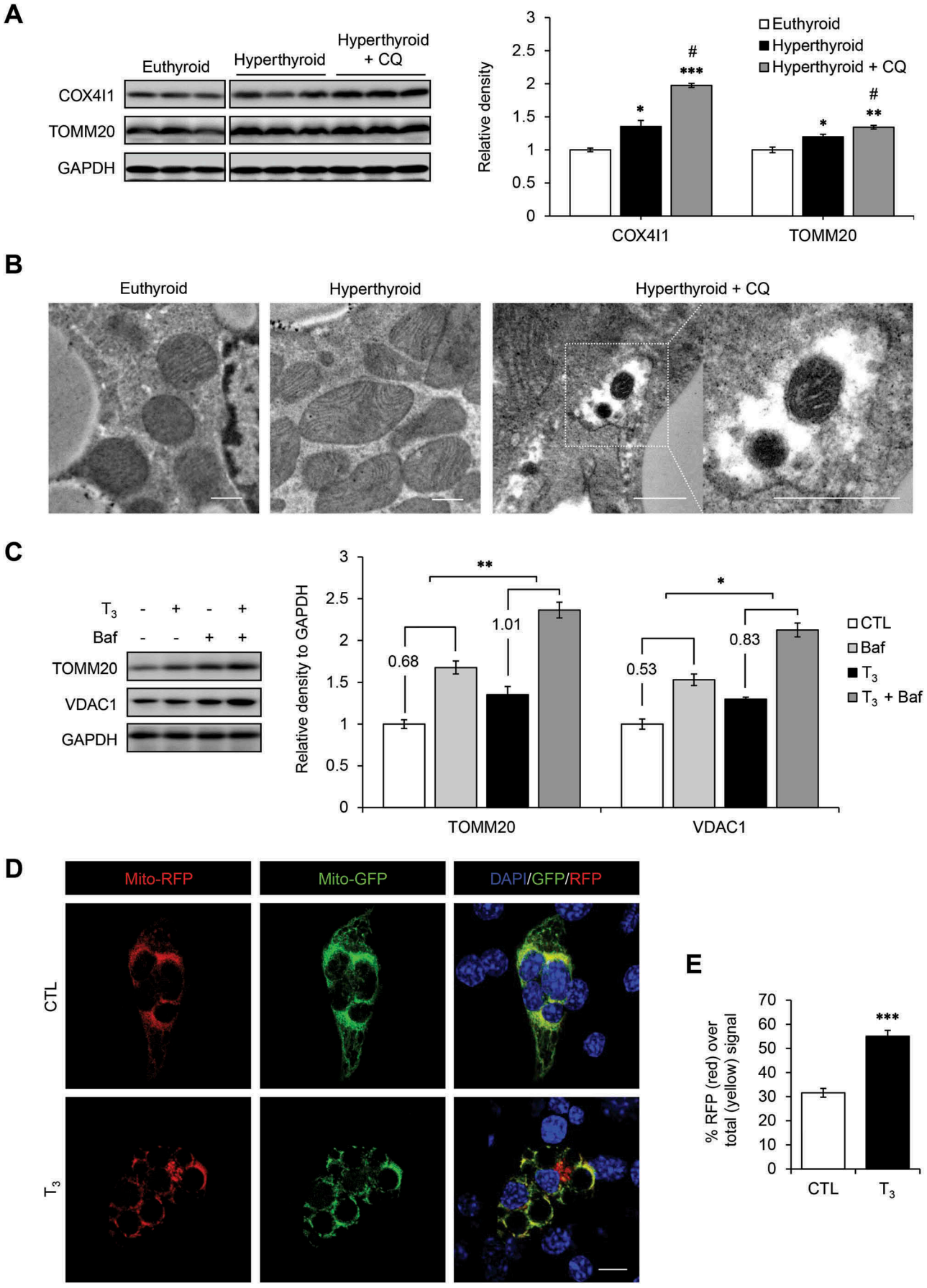

Figure 2. T_3 induces mitophagy in BAT and primary adipocytes. (a) Immunoblots and densitometry showing COX4I1 and TOMM20 levels relative to GAPDH in BATs of hyperthyroid mice injected with chloroquine (CQ) to block autophagy. The blots were from the same gel but cropped for better presentation (Figure S1). Result

primarily derived from the metabolism of these amino acids. In addition, the higher levels of the long chain acylcarnitines, specifically C16 and C18, in BAT from hyperthyroid mice suggested that there was an increase in long chain fatty acid levels due to WAT and BAT lipolysis induced by T_3. Thus, this increase in long chain fatty acid and acylcarnitine levels provided the necessary fuel to sustain increased fatty acid β-oxidation by BAT in hyperthyroid animals (Figure 4(b)).

We next examined the cell autonomous effects of T_3 on BAT mitochondria respiration by using Seahorse analyses to measure oxygen consumption rate (OCR) of primary brown adipocytes treated with T_3 (Figure 4(c)). We found that 24 h of T_3 treatment increased basal OCR and maximum respiratory capacity in primary brown adipocytes in a dose-dependent manner (Figure 4(d)). Interestingly, mitochondrial respiration was upregulated after acute T_3 treatment for 30 min (Figure 4(e,f)), suggesting that T_3 also may have non-transcriptional effects on brown adipocytes. Taken together, our data showed that T_3 was able to activate brown adipocytes in a cell autonomous manner.

T3 stimulates mitochondrial respiration without significant intracellular ROS generation or AMPK activation

We have previously shown that T_3 increases mitochondrial ROS which leads to AMP-activated protein kinase (AMPK) activation and the induction of autophagy in liver and muscle [26,27]. Accordingly, we investigated ROS production and AMPK activation in BAT from hyperthyroid mice by measuring the amount of carbonyl proteins in BAT from euthyroid and hyperthyroid mice. Surprisingly, BAT from hyperthyroid mice showed no significant increase in carbonyl proteins despite having higher mitochondrial activity (Figure S3(a)). Similarly, T_3 treatment did not increase carbonyl proteins in primary brown adipocytes (Figure S3(b)), in contrast to norepinephrine treatment (Figure S3(c)). In conjunction with the lack of significant intracellular ROS production, there also was no change in phosphorylation levels of both AMPK and its downstream target ACACA/ACC after T_3 treatment (Figure S3(d,e)), suggesting that AMPK was not activated by T_3 in brown adipocytes. Because mitochondrial uncoupling may contribute to ROS and AMPK activation, we also examined the effect of *Ucp1* knockdown on autophagy induction. We found that T_3 was able to induce autophagy in the absence of UCP1 upregulation (Figure S3(f)). Moreover, when an ROS inhibitor, N-acetyl-L-cysteine (L-NAC), was added to primary brown adipocytes, T_3 still was able to induce autophagy (data not shown). Taken together, our results showed that AMPK activation and ROS generation were not necessary for autophagy in BAT.

Autophagy facilitates mitochondrial turnover to confer protection from oxidative stress

To demonstrate the crucial role of mitophagy in maintaining mitochondrial function, we analyzed OCR in primary brown adipocytes in which autophagy was inhibited by *Atg5* siRNA (Figures 5(a,b) and S4(a)) or Baf (Figure S4(b,c)). Both treatments blocked the T_3-mediated increase in basal oxygen consumption and maximum respiratory capacity. Interestingly, increased carbonyl protein formation was observed in T_3-treated primary brown adipocytes cells transfected with *Atg5* siRNA or treated with Baf compared to controls (Figure 5(c,d)). Since the lack of ROS induction despite high levels of mitochondrial respiration and UCP1 expression by T_3 was unexpected, we examined the mRNA expression of antioxidant enzymes after T_3 treatment. Surprisingly, there was no induction of antioxidant enzyme mRNAs when primary brown adipocytes were treated with T_3 for 24 h (Figure 5(e)), the same time period when autophagy (Figure 1(e)) and mitochondrial activity (Figure S4(b)) were highly stimulated by T_3. However, they all were significantly induced when autophagy was blocked by Baf (Figure 5(e)). These findings suggested that mitophagy played a major role in maintaining mitochondrial quality control by preventing the accumulation of intracellular ROS in brown adipocytes treated with T_3 as the mRNA expression of antioxidant enzymes increased only when autophagy was blocked.

Induction of thermogenesis in vivo by T_3 requires BAT-specific autophagy

To investigate role of autophagy on thermogenesis *in vivo*, we generated BAT-specific *Atg5* conditional knockout mice (*Atg5* cKO) by injecting *Ucp1* promoter-driven *Cre*-expressing adeno-associated virus into $Atg5^{Flox/Flox}$ mice (Figures 6(a) and S5). In control mice injected with control adenovirus, hyperthyroid mice receiving daily T_3 injection for 10 d exhibited significantly higher body temperature than euthyroid mice. In contrast, hyperthyroid *Atg5* cKO mice exhibited a lower body temperature than control hyperthyroid or euthyroid mice (Figure 6(b)), suggesting that BAT autophagy was important in T_3-mediated thermogenesis. Additionally, hyperthyroid *Atg5* cKO mice had accumulation of protein carbonyls (Figure 6(c)) and deformed mitochondria (Figure 6(d)) suggesting that autophagy was necessary in order to maintain the integrity of BAT mitochondria during thermogenesis.

T_3 induces autophagic flux via the MTOR pathway

Autophagy is inhibited by the MTOR (mechanistic target of rapamycin kinase) pathway through the phosphorylation of

←

represents mean ± SD (n = 3). (b) Electron microscopy images showing mitochondria inside autophagic vesicles in CQ-treated hyperthyroid BATs. Scale bar: 0.5 µm. (c) Representative blots and quantification showing accumulation of TOMM20 and COX4I1 in T_3-treated primary brown adipocytes after autophagy inhibition. Cells were treated 10 nM T_3 for 24 h, followed by 50 nM Baf treatment 6 h before harvest. Result shows mean ± SD (n = 3) where n represents number of independent experiments. (d) Confocal images showing mBAP-9 cells transiently transfected with mito-RFP/GFP plasmid and treated with 10 nM T_3 for 24 h. Yellow color represents normal cytosolic mitochondria. Red color represents mitochondria inside lysosomes. Scale bar: 10 µm. (e) Quantitative analysis of RFP (red) fluorescence over total (yellow) signal to represent relative mitophagy. ImageJ software was used for quantification (at least 10 transfected cells per each sample in 3 different fields). Result shows mean ± SD. *: $P < 0.05$, **: $P < 0.01$ ***: $P < 0.001$ compared to control. #:$P < 0.05$ compared to T_3-treated group.

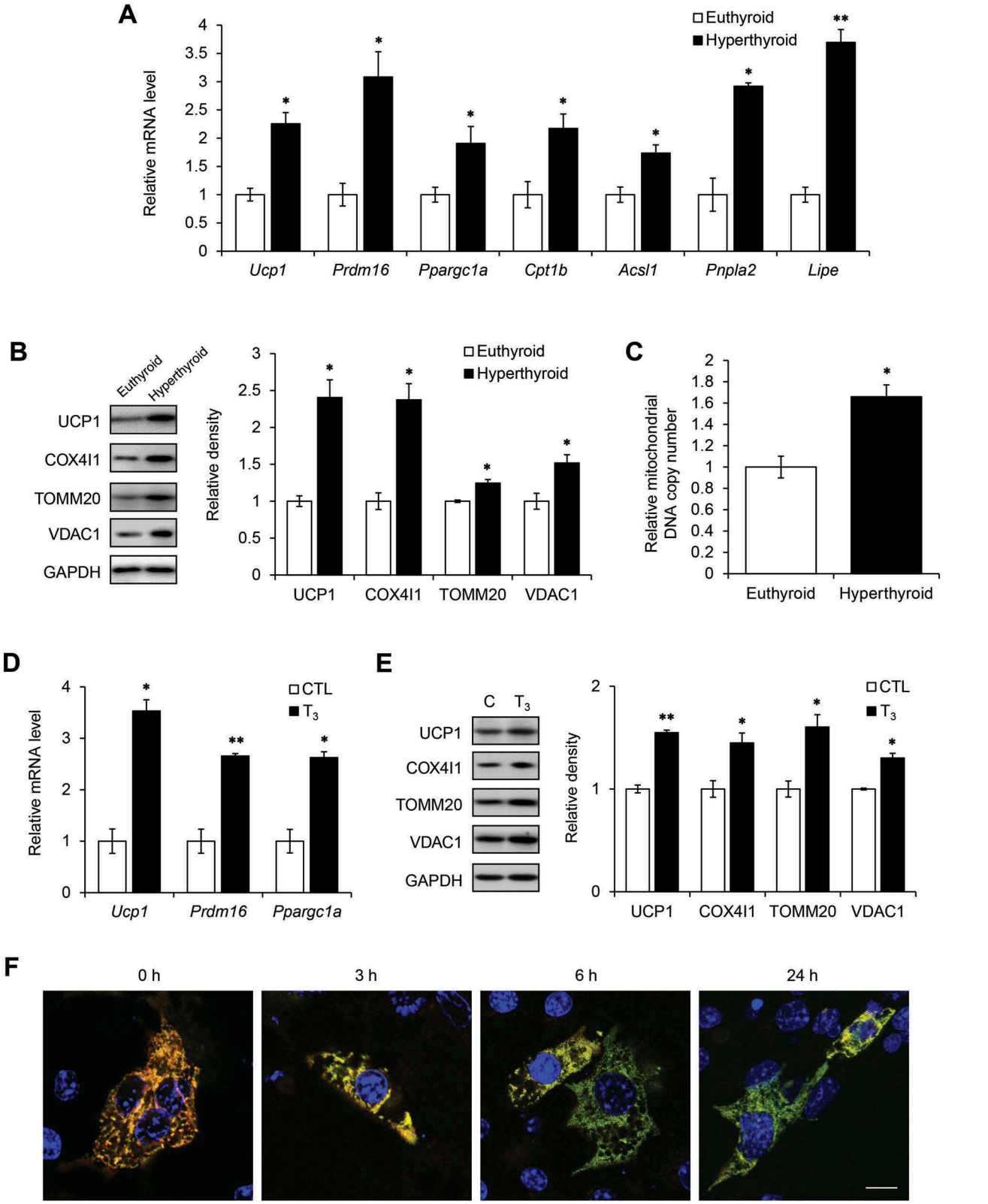

Figure 3. T_3 increases mitochondrial biogenesis and turnover in BAT and primary brown adipocytes. (a) Real time PCR analysis of mRNA levels of *Ucp1*, *Prdm16*, *Ppargc1a*, *Cpt1b*, *Acsl1*, *Pnpla2* and *Lipe* in BATs from hyperthyroid mice using *Polr2a* as the internal control. Result represents mean ± SEM (n = 5). (b) Representative blots and densitometry showing expression levels of COX4I1, TOMM20 and VDAC1 relative to GAPDH in hyperthyroid BATs. Bar represents mean ± SD (n = 3). (c) Graph showing increased mitochondrial DNA copy number in hyperthyroid BAT. Bar represents mean ± SEM (n = 5). (d) Real time PCR analysis of transcript levels of *Ucp1*, *Prdm16* and *Ppargc1a*. Primary brown adipocytes were treated with 10 nM T_3 for 24 h. Bar represents mean ± SD (n = 6) where n represents number of independent experiments. (e) Representative immunoblots and quantification showing expression levels of COX4I1, TOMM20 and VDAC1 relative to GAPDH in cells treated with 10 nM T_3 for 24 h. Result represents mean ± SD (n = 3) where n represents number of independent experiments. *: $P < 0.05$, **: $P < 0.01$, ***: $P < 0.001$. (f) Confocal images showing brown adipocyte cell line mBAP-9 transfected with pMitoTimer plasmid for 72 h. Green represents newly synthesized mitochondria. Red represents mature mitochondria. At indicated time periods before harvest, cells were treated with 10 nM T_3. Scale bar: 10 μm.

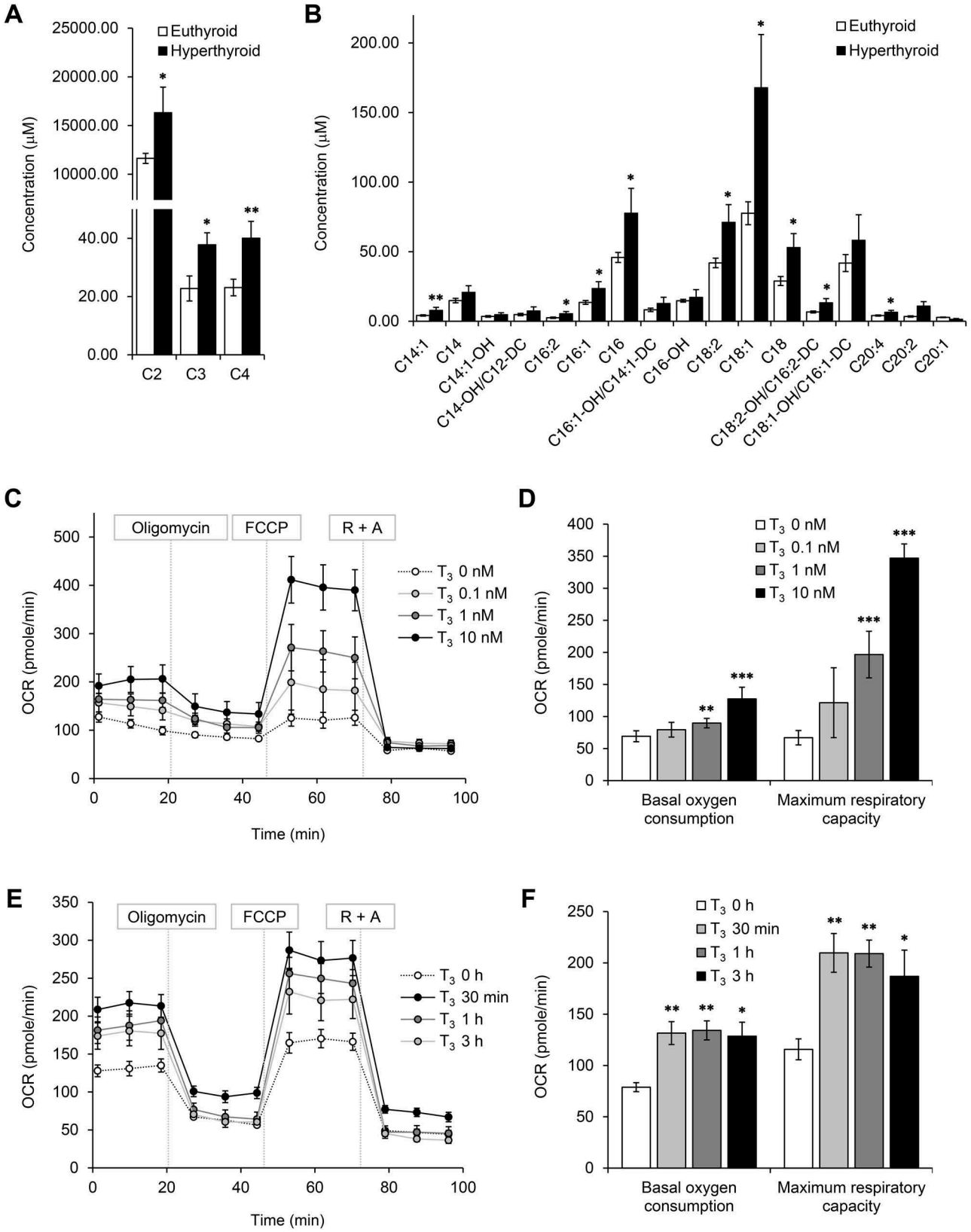

Figure 4. T_3 increases fatty acid oxidation and oxygen consumption in BAT and primary brown adipocytes. Metabolomic profiling of acylcarnitine levels in BATs. Graphs showing concentrations of (a) short chain and (b) long chain acylcarnitines in BATs from hyperthyroid mice. Result represents mean ± SEM (n = 6) (c, d) Seahorse analysis of oxygen consumption rate (OCR) for primary brown adipocytes treated with various doses of T_3 for 24 h. OCR was measured continuously throughout the experimental period at baseline and in the presence of the indicated drugs: 1 μM oligomycin, 1 μM FCCP and 1 μM rotenone with 1 μM antimycin A (R + A). (e) Seahorse analysis of OCR for primary brown adipocytes treated with 10 μM of T_3 for 30 min, 1 and 3 h (f) Graphs showing basal and maximal OCR at different concentrations of T_3. Basal OCR denotes [OCR without inhibitor – OCR with rotenone and antimycin A (R + A) injection]. Maximal OCR or respiratory capacity is calculated by [OCR after FCCP injection – OCR with R + A injection]. Result shows mean ± SD (n = 6) where n represents number of independent experiments. *: $P < 0.05$, **: $P < 0.01$, ***: $P < 0.001$.

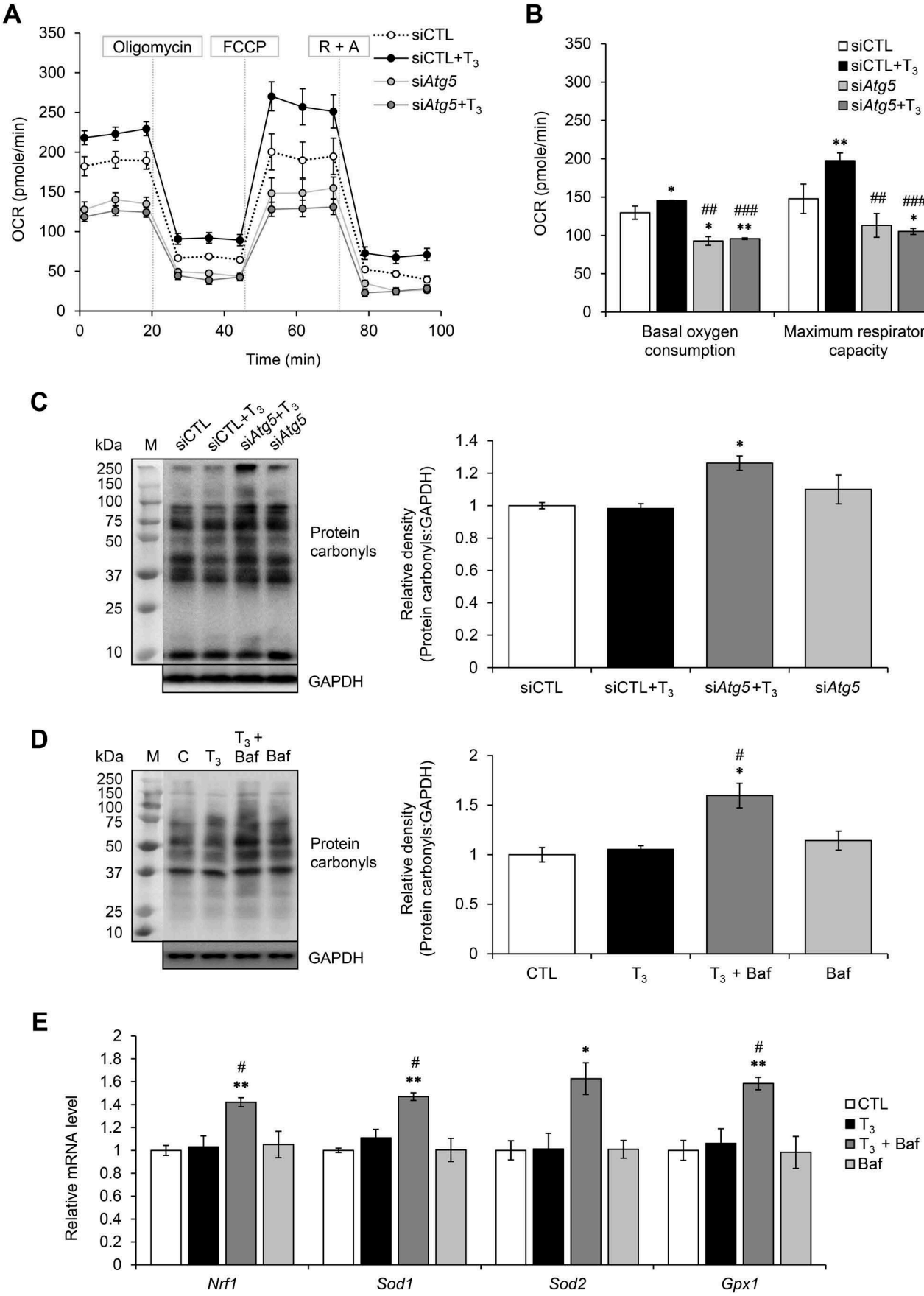

Figure 5. Autophagy inhibition led to increased oxidative stress and reduces mitochondrial activity in primary brown adipocytes. (a) Seahorse analysis of OCR for primary brown adipocytes transfected with control (siCTL) or *Atg5* siRNA (si*Atg5*) for 48 h and treated with or without 10 nM T_3 for 24 h. (b) Graphs showing basal and maximal OCR of *Atg5* siRNA transfected primary brown adipocytes treated with or without 10 nM T_3. Result shows mean ± SD (n = 6) where n represents number of independent experiments. (c) Representative immunoblots and quantification showing protein carbonylation in primary brown adipocytes. Cell were

transfected with *Atg5* siRNA for 48 h and treated with or without 10 nM T_3 24 h before harvest. Bar represents mean ± SD (n = 3) where n represents number of independent experiments. (d) Representative immunoblots and quantification showing protein carbonylation in primary brown adipocytes treated with 10 nM T_3 for 24 h. Baf was added 6 h before harvest (Baf). Bar represents mean ± SD (n = 3) where n represents number of independent experiments. (e) Quantitative PCR result showing mRNA level of antioxidant proteins *Nrf1, Sod1, Sod2* and *Gpx1* using *Polr2a* as the internal control. Cell were treated with 10 nM T_3 for 24 h with or without Baf. Bar represents mean ± SD (n = 3) where n represents number of independent experiments. *: $P < 0.05$, **: $P < 0.01$, ***: $P < 0.001$ compared to control. #: $P < 0.05$, ##: $P < 0.01$, ###: $P < 0.001$ compared to T_3-treated group.

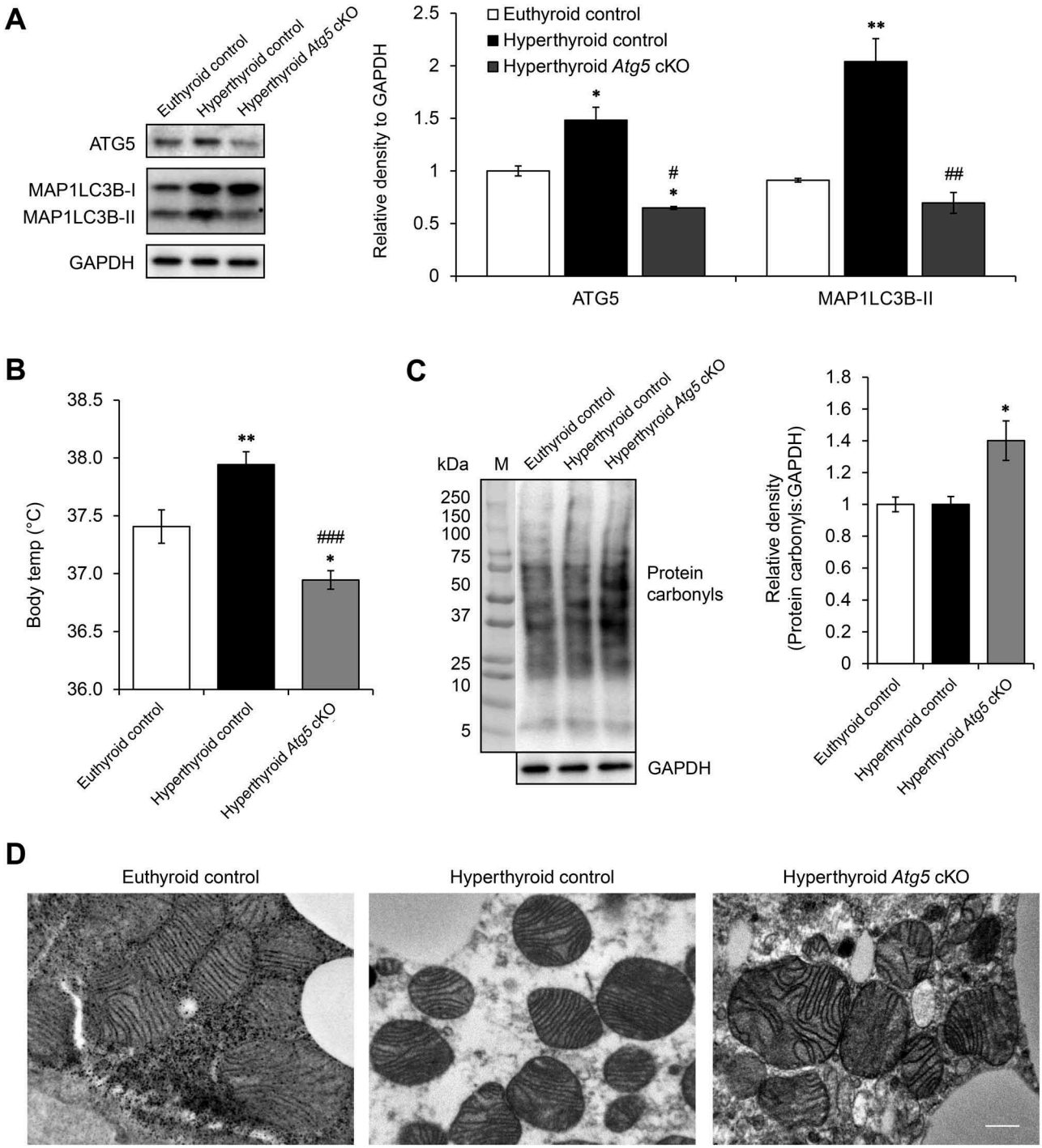

Figure 6. BAT-specific autophagy inhibition abolished T_3-mediated thermogenesis. (a) Representative immunoblots and quantification showing decrease in ATG5 and MAP1LC3B-II level in BAT of *Atg5* cKO mice. Bar represents mean ± SEM (n = 3). (b) Graph shows body temperature of control and *Atg5* cKO and made hyperthyroid by daily T_3 injection for 10 d. Result shows mean ± SEM (n = 3). (c) Representative immunoblots and quantification showing increased protein carbonyls in BAT of hyperthyroid *Atg5* cKO mice. Bar represents mean ± SEM (n = 3). *: $P < 0.05$, **: $P < 0.01$ compared to control. #: $P < 0.05$, ##: $P < 0.01$, ###: $P < 0.001$ compared to T_3-treated group. (d) Electron microscopy images showing distorted mitochondria in hyperthyroid *Atg5* cKO mice. Scale bar: 0.5 µm.

ULK1 by activated MTOR complex 1 (MTORC1). Since neither AMPK nor ROS played significant roles in the activation of autophagy by T_3 in BAT, we examined MTORC1 activity. Interestingly, we observed a decrease in MTOR and EIF4EBP1 phosphorylation in BAT from hyperthyroid mice (Figure 7(a)). Similarly, T_3 decreased the level of

phosphorylated MTOR and the 2 MTORC1 targets, RPS6KB and EIF4EBP1 in a time-dependent manner in primary brown adipocytes (Figure 7(b)). Inhibition of MTOR was independent of mitochondrial uncoupling since T_3 was able to reduce phosphorylation of RPS6KB in brown adipocytes transfected with siRNA targeting *Ucp1* (Figure S6(a)). Moreover, inhibition of MTOR led to increased nuclear translocation of TFEB (transcription factor EB) (Figure S6(b)), a master regulator of autophagy and lysosomal target genes. This effect on TFEB in BAT by T_3 increased the mRNA expression of the TFEB target genes involved in autophagy such as *Atg5* and *Atg7* (Figure S6(c)). Since MTORC1 is a nutrient sensor and its activity is regulated by amino acid content, we next performed amino acid profiling in hyperthyroid BAT. Interestingly, we found that T_3 reduced the intracellular BAT levels of a broad range of amino acids (Figure 7(c)), particularly leucine and

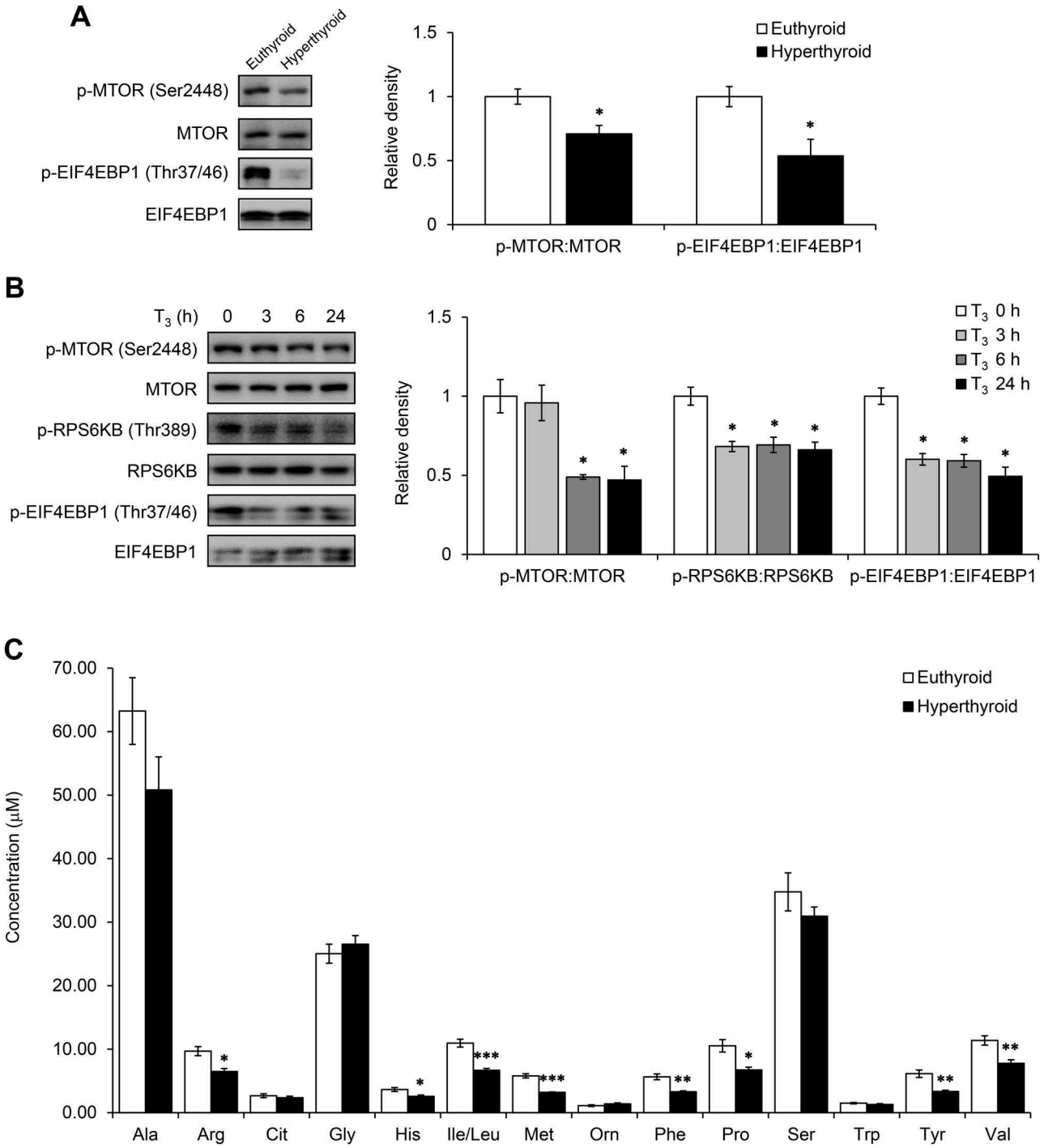

Figure 7. T_3 inhibited MTOR in BAT and primary adipocytes. (a) Representative blots and quantification showing levels of phosphorylated MTOR and its downstream target EIF4EBP1 in BATs of hyperthyroid mice. Result represents mean ± SEM (n = 3). (b) Representative blots and densitometry showing levels of phosphorylated MTOR, RPS6KB and EIF4EBP1 in primary brown adipocytes treated with 10 nM T_3 for 0, 3, 6 and 24 h. Result represents mean ± SD (n = 3) where n represents number of independent experiments. (c) Graph showing amino acid profile in hyperthyroid BAT. Result represents mean ± SEM (n = 6). *: $P < 0.05$, **: $P < 0.01$, ***: $P < 0.001$ compared to euthyroid BAT.

arginine, which previously have been shown to stimulate MTORC1 activity in adipocytes [30–32]. These findings also were consistent with our acylcarnitine metabolomics analysis (Figure 4(a)) in which we observed increased C2 and C3 acylcarnitine levels. Both these species are end products and markers of amino acid oxidation.

SIRT1 regulates MTOR activity and T_3-mediated autophagy

Because we have previously reported that T_3 increases SIRT1 activity in hepatocytes, we also examined SIRT1 activity in brown adipocytes. SIRT1 is an NAD^+-dependent deacetylase which has been reported to facilitate browning and BAT activity [33]. One of its downstream targets is FOXO1 (forkhead box O1), which regulates the expression of a number of autophagy related genes including *Map1lc3b* and *Sqstm1*. BAT from hyperthyroid mice had decreased acetylation of FOXO1 compared to BAT from euthyroid mice (Figure 8(a)), suggesting that T_3 treatment activated SIRT1 and deacetylated FOXO1 in BAT. Accordingly, we observed that FOXO1 target genes (*Map1lc3b, Sqstm1 and Pck1)* were upregulated in BAT from hyperthyroid mice. We also observed the same trend *in vitro* as T_3 reduced FOXO1 acetylation (Figure 8(c)), increased NAD^+:NADH ratio (Figure 8(d)) and upregulated FOXO1 target genes in a time-dependent manner (Figure 8(e)) in primary brown adipocytes. We also examined whether SIRT1 acts upstream of MTORC1 since SIRT1 previously has been reported to negatively regulate MTORC1 activity [34]. Inhibition of SIRT1 activity by EX527 abolished T_3-mediated MTOR inhibition and autophagy induction (Figures 8(f) and S7). Moreover, inhibiting SIRT1 activity by EX527 abolished the induction of mitochondrial respiration by T_3 in brown adipocytes (Figure 8(g,h)) and confirmed that SIRT1 activity and autophagy induction were important for mitochondrial function.

Discussion

Thyroid hormone activates non-shivering thermogenesis by increasing metabolic activity in BAT. Hypothyroid patients have decreased adaptive thermogenesis during cold exposure that is corrected by thyroid hormone replacement [35] whereas hyperthyroid patients can undergo activation of thermogenesis, even at room temperature [36]. During cold exposure, sympathetic stimulation of BAT increases DIO2 expression and raises intracellular T_3 concentration [5,37]. Christoffolete et al. have established that T_3 is necessary for activation of thermogenesis in BAT since lack of adipose DIO2 causes abnormal lipid metabolism in BAT that eventually leads to cold intolerance despite increased sympathetic induction of UCP1 expression [10]. Previous studies have suggested that thyroid hormone mediates its effects on BAT primarily via hypothalamic stimulation of sympathetic innervation and induction of DIO2 expression [14,15]; however, a cell autonomous role of thyroid hormone on BAT activity has not been clearly established. Accordingly, we examined the metabolic role of T_3-mediated autophagy on BAT function in a BAT cell line, primary brown adipocytes, and *in vivo* at normal temperature to eliminate the confounding effects of cold-induced sympathetic innervation. We refer to this increase in BAT activity at room temperature as 'activated' thermogenesis rather than adaptive thermogenesis since the latter occurs during cold exposure. In WAT, autophagy facilitates triglyceride accumulation and adipogenesis [38], and adipose-specific ablation of autophagy during development can lead to a browning phenotype [23]. Since these mice have increased whole body oxygen consumption and energy utilization, it is likely that the extensive browning in inguinal white fat due to inhibition of autophagy plays an important role in altering their metabolism and metabolic rate [23]. Additionally, it recently has been shown that a thyroid hormone analog, GC-1, can transdifferentiate WAT to beige fat [39]; however, little is known about the role of autophagy during this process. Inhibition of autophagy has been reported to facilitate browning of WAT and activation of autophagy has been associated with beige-to-white transition of adipocytes after withdrawal of external stimuli [40,41]; however, the role of autophagy in mature BAT had not been examined previously.

T_3 stimulates BAT activity in a cell-autonomous manner

T_3 stimulates thermogenesis by increasing transcription of *Ucp1* and lipid metabolism in BAT [5,10]. Several recent studies show a central role for T_3 in the hypothalamus and suggest that sympathetic stimulation was the main driver to increase BAT activity by inducing lipolysis and mitochondrial uncoupling [14,42]. However, while sympathetic activation significantly induces expression of DIO2 which generates T_3 [14,15,43], the role of intracellular T_3 on BAT activity has not been clearly established. Here, we showed that instead of merely playing a permissive role, T_3 itself was sufficient for BAT and brown adipocyte activation since T_3 increased acylcarnitine flux *in vivo* at room temperature. It also rapidly induced mitochondrial respiration in primary brown adipocytes in cell culture (30 min) suggesting that a non-transcriptional mechanism may be involved in stimulating mitochondrial activity initially (Figure 4(e,f)). Of note, we found that T_3 increased PRKA activity and phosphorylation of PNPLA2 *in vivo* (Figure S8), suggesting that the sympathetic system also was activated by T_3. Thus, it is likely that both local and central effects contribute to the BAT activation by T_3.

T_3 induces mitophagy, mitochondrial biogenesis and mitochondrial turnover in BAT

It has been speculated that autophagy may have an important functional role in BAT based upon studies in *Fabp4*- or *Myf5*-associated, tissue-specific *Atg7* knockout mouse models [23,44]. Mice with *Fabp4*-associated (adipose tissue specific) deletion of the *Atg7* gene had more mitochondria in both white and brown adipose tissues [23], suggesting that autophagy was essential for mitochondrial clearance. Moreover, BAT from mice with *Myf5*-associated (BAT and skeletal muscle specific) *Atg7* conditional gene deletion exhibited

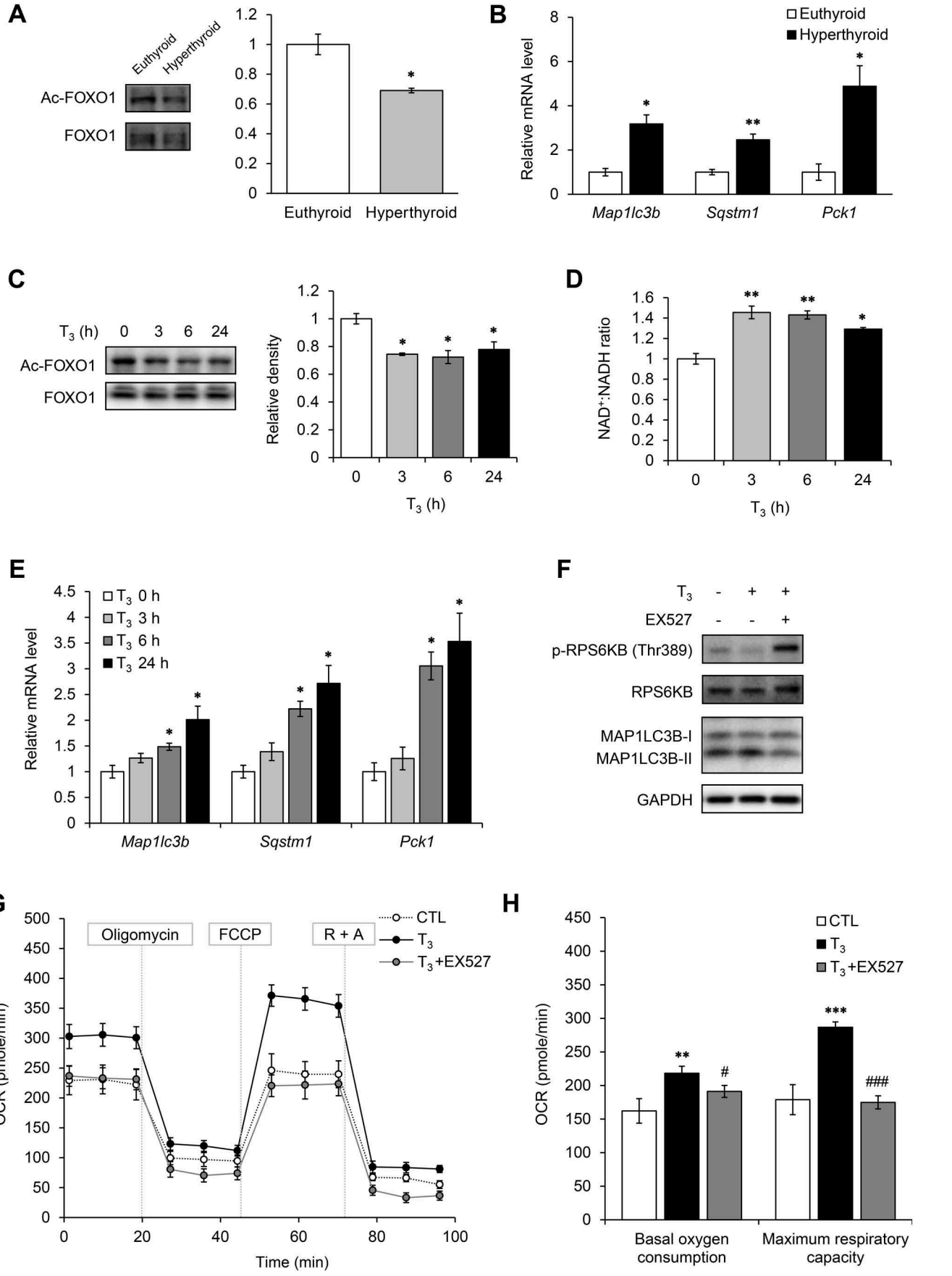

Figure 8. T_3 activated SIRT1 in BAT and primary adipocytes. (a) Representative blots and quantification showing levels of acetylated FOXO1 in BAT of hyperthyroid mice. Result represents mean ± SEM (n = 3). (b) Real time PCR analysis of mRNA levels of FOXO1 target genes (*Map1lc3b, Sqstm1* and *Pck1*) in BAT. Result represents mean ± SEM (n = 5). (c) Representative blots and densitometry showing levels of acetylated FOXO1 in primary brown adipocytes treated with 10 nM T_3 for 0, 3, 6 and 24 h. Result represents mean ± SD (n = 3) where n represents number of independent experiments. (d) Graph showing NAD^+/NADH ratio in primary brown

adipocytes treated with 10 nM T_3 for 0, 3, 6 and 24 h. Result represents mean ± SD (n = 6) where n represents number of independent experiments. (e) Real time PCR analysis of mRNA levels of FOXO1 target genes (*Map1lc3b, Sqstm1* and *Pck1*) in primary brown adipocytes adipocytes treated with 10 nM T_3 for 0, 3, 6 and 24 h. Result represents mean ± SD (n = 6) where n represents number of independent experiments. (f) Effect of SIRT1 inhibitor on T_3-induced MTOR inhibition and autophagy. Representative immunoblots showing levels of RPS6KB phosphorylation and MAP1LC3B-II in primary brown adipocytes treated with EX527 and T_3 for 6 h. (g) and (h) Seahorse analysis of OCR for primary brown adipocytes transfected with treated with EX527 and T_3 for 24 h. Result represents mean ± SEM (n = 5) where n represents number of independent experiments. *: $P < 0.05$, **: $P < 0.01$, ***: $P < 0.001$ compared to euthyroid BAT.

deformed mitochondria with distorted cristae, further suggesting the importance of autophagy in BAT function [44].

In our studies, we showed that T_3 stimulated autophagy in a cell-autonomous manner. T_3 also induced autophagy and autophagic flux in primary brown adipocytes and BAT from hyperthyroid mice. Additionally, we showed that T_3 stimulated mitophagy in BAT, using multiple methods including assessment of mitochondrial protein accumulation when autophagy was blocked, electron microscopy and mito-RFP/GFP fluorescence studies. Our mitochondria fractionation studies showed that T_3 increased localization of SQSTM1 and MAP1LC3B-II in mitochondria (Figure S2(b,c)), suggesting that there was active recruitment of autophagy proteins to the mitochondria.

T_3 induces mitochondrial biogenesis and respiration in liver and skeletal muscle [26,27], and lack of T_3 impairs mitochondrial biogenesis during BAT development [9]. In our study, we showed that T_3 stimulated the expression of PPARGC1A as well as several mitochondrial proteins in a cell autonomous manner (Figure 3). It also increased β-oxidation of fatty acids and mitochondrial respiration in BAT and primary brown adipocytes (Figure 4). These findings strongly suggested that efficient mitophagy coupled with increased mitochondrial biogenesis played a major role in increasing mitochondrial activity and thermogenesis. In this connection, we also observed high mitochondrial turnover rate by T_3 by MitoTimer analysis (Figure 3(f)). Since T_3 increased net mitochondrial number and activity in BAT and primary brown adipocytes, it suggested that T_3 induced mitochondrial biogenesis at a higher rate than degradation. Additionally, unlike BAT in *Atg5* (Figure 6) or *Atg7* [44] conditional knockout mice, we did not observe gross deformities in mitochondrial architecture in BAT from the hyperthyroid mice, which again highlights the efficiency of mitochondrial turnover induced by T_3.

T_3 induces autophagy by inhibiting MTOR

We have previously shown that there is a tight coupling between autophagy and mitochondrial biogenesis in skeletal muscle [27]. This coupling was mediated by ROS generated from active mitochondria and involved AMPK stimulation of autophagy and mitochondrial biogenesis via ULK1 and PPARGC1A phosphorylation, respectively. Since T_3 increases mitochondrial uncoupling and activity in brown adipocytes, we hypothesized that it may lead to ROS generation followed by AMPK activation. However, in contrast to our findings in liver and skeletal muscle [26,27], ROS and AMPK did not play a significant role in T_3-induced autophagy in BAT since T_3 did not increase amount of carbonyl proteins or significantly change AMPK phosphorylation (Figure S3). Instead, we observed that T_3 inhibited MTOR activity, which is known to stimulate autophagy (Figure 6(a,b)). Knockdown of *Ucp1* also did not prevent MTOR inhibition or autophagy induction by T_3 (Figures S3(f) and S6(a)). Moreover, quenching ROS production with L-NAC did not suppress T_3-mediated autophagy in BAT (data not shown), further suggesting that ROS was not responsible for the induction of autophagy in BAT. The ROS-independent activation of autophagy in BAT by T_3 contrasted with our previous findings in liver and muscle from hyperthyroid mice, in which induction of mitophagy by T_3 is activated by ROS, which then leads to increased intracellular calcium to stimulate CAMKK (calcium/calmodulin-dependent protein kinase kinase), followed by activation of AMPK, and AMPK phosphorylation of ULK1 to initiate phagophore formation [26,27]. In contrast, induction of autophagy in BAT by T_3 was not initiated by ROS or AMPK activation, but instead, it was more likely caused by a decrease in MTOR activity.

T_3 inhibits MTOR activity by amino acid catabolism and SIRT1 activation

BAT exhibits high amino acid handling capacity [45] and can employ amino acids as alternative sources of metabolic substrates during acute cold exposure [46]. Using metabolomic analyses, we showed that T_3 decreased BAT amino acid levels due to stimulation of amino acid catabolism (Figures 4(a) and 7(c)). This, in turn, inhibited MTOR activity in BAT. We showed that T_3 induced expression of PPARGC1A (Figure 3(a,d)), which is responsible for catabolism of branched chained amino acids (leucine, isoleucine and valine) in skeletal muscle [47]. Additionally, we also saw an increase in C3 acylcarnitine levels arising from oxidation of these amino acids. These data strongly suggest that T_3 caused BAT to utilize amino acids as an additional fuel source in addition to fatty acids. It currently is not clear whether decreases in specific amino acids or total amino acids directly stimulated MTOR. Interestingly, leucine, glutamine and arginine previously were implicated in MTOR activation [31,32] and since the levels of leucine and arginine were significantly reduced in BAT from hyperthyroid mice, the decrease in these amino acids may have contributed to the decreased MTOR activity in this tissue. Although MTOR inhibition may be the main contributor to autophagy in BAT from hyperthyroid mice, it is possible that other upstream signalling pathways also contributed to MTOR inhibition. In particular, it is possible that UCP1-independent mitochondrial uncoupling also could have contributed to MTOR inhibition and/or autophagy, since mild mitochondrial uncoupling by FCCP induced autophagy in adipocytes [48]. In support for

a similar effect by T_3, mitochondrial uncoupling was able to increase OCR within 30 min in brown adipocytes (Figure 4(e)). Moreover, the associated decrease in MTOR activity did require UCP1, and thus was UCP-1 independent (Figure S6(a)). Of note, rapid and non-transcriptional effects by T_3 on mitochondria have been reported to involve its direct binding to mitochondria [49]. This uncoupling effect also was not restricted to brown adipocytes since we previously observed acute OCR induction (1 h) by T_3 in hepatocytes [26]. Acute mitochondrial uncoupling appears to be an early phase of autophagy induction that precedes transcriptional activation of autophagy genes by FOXO1 or TFEB. Although increased mitochondrial uncoupling by T_3 in BAT did not induce ROS and AMPK activity, it can increase NAD^+/NADH ratio and activate SIRT1. We have previously shown that T_3 activates SIRT1 [50], a NAD^+-dependent histone deacetylase that is a negative regulator of MTOR [34], in hepatocytes. Consistent with its ability to increase mitochondrial respiration and uncoupling, T_3 also increased intracellular NAD^+/NADH and activated SIRT1 within 3 to 6 h in BAT and primary brown adipocytes as well as liver [50] (Figure 7(d)). Interestingly, T_3 was unable to decrease MTOR activity, induce autophagy, or increase oxidative phosphorylation when SIRT1 was inhibited (Figure 8(f,g,h)), suggesting that T_3-mediated MTOR inhibition and autophagy in BAT required SIRT1. Since SIRT1 also can be activated by the cAMP-AMPK pathway [51], it may play a role in early autophagy induction when there is sympathetic stimulation of BAT. Although the relative contributions of decreased amino acids, SIRT1 activation, or other upstream signalling mechanism(s) on MTOR inhibition by T_3 are not known; nevertheless, our data strongly imply that early T_3-mediated stimulation of autophagy required MTOR inhibition whereas longer term autophagy may also require increased expression of autophagy genes.

Lipase may provide fatty acids to mitochondria during BAT activation by T_3

The physiological significance of autophagy on BAT activation by thyroid hormone has not been characterized previously. Recently, Martinez-Lopez et al. report that cold exposure or sympathetic stimulation acutely induces lipophagy in BAT to undergo lipolysis of stored triglycerides to generate fuel for fatty acid β-oxidation [25]. While it certainly is possible that T_3 also induced lipophagy, we did not find either increased lipid-laden autophagosomes in EM or colocalization of BODIPY and MAP1LC3B in BAT, in contrast to our previous observations in liver and muscle [26,27]. During classical lipolysis, free fatty acids are generated from endogenous triglycerides by protein kinase A-activated lipases such as PNPLA2/ATGL. In this connection, T_3 stimulated mRNA expression (Figure 3(a)) and protein kinase A-mediated phosphorylation (Figure S8) of PNPLA2 in BAT to stimulate lipase activity. Taken together, it appears that classical lipolysis may play a more significant role than lipophagy in generating fatty acids as fuel for β-oxidation in BAT.

Both cold exposure and thyroid hormone increase autophagy and BAT activity

Cold exposure is the primary stimulus for adaptive thermogenesis, but the involvement of autophagy during BAT activation remains unclear. A recent study shows that one day of cold exposure leads to inhibition of autophagy in BAT accompanied by accumulation of mitochondria and UCP1 proteins [52]. However, Martinez-Lopez et al. show that activation of lipophagy in BAT after 1 h of acute cold exposure [25]. Thus, regulation of autophagy in BAT may be governed by the duration of cold exposure and the temporal response to different hormones. Accordingly, we examined autophagy and temporal expression of autophagy genes in mice during cold exposure and found that autophagy was blocked after one day; however, both transcription and expression of autophagy proteins are induced and autophagy is increased after 3 d of cold exposure (Yau and Yen, unpublished data). In this connection, it is reported that mitochondrial function during cold exposure is decreased in mice with adipose tissue-specific impairment of autophagy (adenovirus with BAT-specific *Cre* into $Atg7^{Flox/Flox}$ mice) [44]. Similarly, our study in *Atg5* cKO mouse model showed decreased body temperature in hyperthyroid *Atg5* cKO mice, further confirming the importance of autophagy during BAT activation. Since cold exposure increases expression of DIO2 in BAT [53,54], it is likely that stimulation of BAT autophagy and mitochondrial clearance in cold-acclimated mice may be facilitated by increased generation of intracellular T_3 by DIO2 [1,5,15]. Our study also showed that T_3-stimulated autophagy prevented oxidative stress in BAT. Blocking autophagy increased oxidative stress and decreased brown adipocyte mitochondrial respiration. Significantly, ROS and ROS-induced cellular damage previously have been observed in BAT mitochondria during cold exposure [55–57], so it is possible that mitochondrial respiration and consequent ROS generation may be higher for cold exposure than for T_3 treatment. Taken together, we showed that autophagy in BAT is important for regulating mitochondrial function during thermogenesis and T_3 likely facilitates the induction of autophagy and mitochondrial turnover during BAT activation.

Conclusion

Recent reports have suggested that BAT activation may have potential beneficial effects in reducing obesity and improving glycemic control in diabetes [7]. In a recent human study, Cypess et al. show that a β3-adrenergic receptor agonist can activate BAT [58]. Broaeders et al. report that levothyroxine treatment improves human BAT activation in response to cold [35]. Thyromimetics that specifically target BAT may be useful for pharmacological activation of BAT [39] while potentially have less side effects than TH. These analogs have therapeutic promise for the treatment of obesity and other metabolic diseases since they are able to stimulate BAT activity at normal temperatures.

Our results demonstrated that T_3 has a cell autonomous role in BAT thermogenesis by stimulating autophagy-dependent fatty acid oxidation and mitochondrial respiration. These

effects were coupled to increased mitochondrial biogenesis, mitophagy, and mitochondrial turnover by T_3. Surprisingly unlike adrenergic stimulation or thyroid hormone effects in the liver and muscle, activation of mitochondrial oxygen consumption by T_3 did not generate high levels of ROS or induce expression of antioxidant enzymes. Instead, BAT relied primarily on increased mitophagy and mitochondrial biogenesis to maintain mitochondrial quality control. Our findings suggest that T_3 and its analogs as well as other autophagy-inducing drugs that promote high mitochondrial turnover in BAT may potentially be useful therapies that increase thermogenesis in BAT to treat obesity and other associated metabolic conditions.

Materials and methods

Reagents

Unless otherwise specified, all chemicals were obtained from Sigma-Aldrich and all culture media were from Gibco (Thermo Fisher Scientific). Transfection reagents and siRNA (Ambion, 4390771) were purchased from Thermo Fisher Scientific. The eGFP-MAP1LC3B (Addgene, 21073) and mito-RFP-EGFP plasmids were kind gifts from Prof. T. Yoshimori (Osaka University, Osaka, Japan) and Dr Andreas Till (Institute of Clinical Molecular Biology Christian-Albrechts-University of Kiel; Kiel, Germany), respectively. pMitoTimer was a gift from Zhen Yan (Addgene, 52659). The CoralHue® Mitochondria-targeted mKeima-Red expression plasmid (pMT-mKeima-Red, AM-V0251) was purchased from MBL International Corporation. Norepinephrine was purchased from Sigma-Aldrich (A0937).

Animals

Animals were treated in accordance with the Guide for the Care and Use of Laboratory Animals and experiments were approved by the Institutional Animal Care and Use Committee (IACUC) and Duke-NUS Graduate Medical School. Male C57BL/6 mice (8 to 10 wk old) were housed in hanging polycarbonate cages and kept on a 12 h light-dark cycle in a temperature-controlled room at 24°C. They were allowed *ad libitum* access to water and a standard laboratory chow. Mice were made hyperthyroid by daily intraperitoneal injection of 10 μg T_3 (Sigma-Aldrich, T6397) per 100 g body weight for 10 d. Autophagy inhibition *in vivo* was achieved by intraperitoneal injection of 6 mg chloroquine (CQ) (Sigma-Aldrich, C6628) per 100 g body weight for 3 d. For cold exposure, mice were housed at 4°C for 3 d.

Adenoviral infection

For tissue-specific knockout study, male homozygous *Atg5*$^{Flox/Flox}$ mice (C57BL/6/129) were obtained from the Riken BioResource Center, Japan, courtesy of Dr. Noboru Mizushima [59,60]. A total of 5×10^{11} genome copies of control adenovirus or *Ucp1-Cre*-expressing adeno-associated virus (Vector BioLabs, AAV8-UCP1-eGFP and AAV8-UCP1-iCre) was injected into tail vein of 10-week-old male *Atg5*$^{Flox/Flox}$ mice. After 2 wk of injection, the mice were made hyperthyroid by daily T_3 injection for 10 d. Core body temperature was measured using a rectal temperature probe on the last day of T_3 injection.

Primary culture of brown preadipocytes

Primary brown adipocytes were derived from the interscapular BAT of 2 to 3 wk old C57BL/6 mice. The precursor cells were isolated according to the protocols described by Rehnmark *et al.* and Klein et al. [61,62]. Briefly, BAT from 6 to 8 mice was cut into small pieces and digested with 0.2% (w:v) collagenase (Sigma-Aldrich, C6885) for 30 min in a shaking water bath. After filtering through a 150-μm nylon screen (Fisher Scientific, 22363549), the pellet containing preadipocytes were collected by centrifugation at 200 g for 5 min. Preadipocytes were maintained in DMEM (Gibco, 11995–065) supplemented with 15% heat inactivated FBS (Gibco, 10500–064), non-essential amino acids (Gibco, 11140–076), 5 ng/ml human basic FGF (Thermo Fisher Scientific, PHG0021), 100 U/ml penicillin and 50 μg/ml streptomycin (Sigma-Aldrich, F7524). Differentiation was initiated with DMEM containing 10% fetal bovine serum (FBS; Gibco, 15140122), dexamethasone (Sigma-Aldrich, D1756), 3-isobutyl-1-methylxanthine (IBMX) (Sigma-Aldrich, I5879) and insulin (Sigma-Aldrich, I9278). Cells were allowed to differentiate for 6 d before treatment. For T_3 treatment, cells were treated with 10 nM T_3 for 24 h unless stated otherwise. For autophagic flux assay, cells were treated with 50 nM bafilomycin A_1/Baf (Sigma-Aldrich, B1793) 6 h before harvest. For RNA interference studies, Lipofectamine® RNAiMAX Reagent (Invitrogen, 13778075) was used to transfect the cells 2 d before T_3 treatment.

Cell line transfection

Plasmid transfection were performed in the brown adipocyte cell line mBAP-9 [63]. Cells were seeded on cell culture slide (SPL Life Sciences, 30104) and maintained in DMEM containing 10% FBS and differentiated by DMEM containing 10% FBS, insulin, T_3, dexamethasone and IBMX for 6 d before treatment. Transfection was carried out 2 d before treatment in medium without T_3 using Lipofectamine® 3000 Reagent (Invitrogen, L3000008) in accordance to the manufacturer's protocols. After transfection, cells were treated with 10 nM of T_3 for 24 h before fixation with 4% paraformaldehyde (Sigma-Aldrich, P6148). Cell imaging was performed using a Zeiss LSM 710 Confocal Microscope.

Western blotting

Cells and tissues were dissociated in RIPA buffer (50 mM Tris-HCl, pH 8.0, 150 mM sodium chloride, 1% Triton X-100 (Bio-Rad, 1610407), 0.5% sodium deoxycholate (Sigma-Aldrich, D6750), 0.1% sodium dodecyl sulfate, 2 mM EGTA, 2 mM EDTA, protease inhibitors (Sigma-Aldrich, P8340) and phosphatase inhibitors (Sigma-Aldrich, P5726, P0044). Proteins were denatured by boiling in Laemmli sample buffer (250 mM Tris-HCl, pH 7.4, 2%

w:v sodium dodecyl sulfate, 25% v:v glycerol, 50 mM DTT, 0.01% w:v bromophenol blue). Equal amount of proteins was resolved on sodium dodecyl sulfate-polyacrylamide gels using the Mini-PROTEAN 3 Electrophoresis unit and transferred to polyvinylidene difluoride membranes (Bio-Rad) using the TransBlot® Turbo™ Transfer System (Bio-Rad). The following antibodies were used to detect the target proteins. Cell Signaling Technology: MAP1LC3B (2775), SQSTM1/p62 (5114), COX4I1 (4850), ATG5 (2630), PRKAA1/2 (protein kinase AMP-activated catalytic subunit alpha 1) (5831), phospho-PRKAA1/2 (Thr172) (2535), MTOR (2983), phospho-MTOR (Ser2448) (5536), RPS6KB (9202), phospho-RPS6KB (Thr389) (9205), EIF4EBP1 (9452), phospho-EIF4EBP1 (Thr37/46) (2855), VDAC1 (4661), FOXO1 (2880), PRKA/protein kinase A substrates (9621) and GAPDH (2118). Santa Cruz Biotechnology: ACTB (sc-47778), TOMM20 (sc-11415) and acetylated FOXO1 (sc-49437), Abcam: UCP1 (ab10983), PNPLA2 (ab99532) and phospho-PNPLA2 (Ser406) (ab135093).

Protein carbonylation

The amount of protein carbonyls was measured with an OxyBlot™ Oxidized Protein Detection Kit (EMD Millipore, S7150) according to the manufacturer's protocol.

Quantitative real-time PCR

Total RNA was isolated using the InviTrap Spin Universal RNA Mini Kit (Stratec Molecular, 1060100300) followed by cDNA synthesis using iScript Select cDNA Synthesis Kit (Bio-Rad, 1708897) according to the manufacturer's protocol. Quantitative polymerase chain reaction was performed on a Rotor-Gene Q cycler (QIAGEN, USA) using QuantiTect SYBR Green PCR Kit (QIAGEN, 204145) in accordance with the manufacturer's instructions using *Polr2a* as the internal control. Sequence of the primers are listed in Table S1.

Seahorse XF analyzer measurement for mitochondrial oxygen consumption rate (OCR)

Preadipocytes were seeded on XF-24-well culture microplates and allowed to differentiate for 7 d. After treatment, oxygen consumption was measured using a microplate (type XF24) extracellular analyzer (Seahorse Bioscience, Billerica, MA, USA). Reagents were optimized using the Mito stress kit from Seahorse Bioscience (Agilent, 100850–001) using the protocol and algorithm program in the analyzer. After measuring initial oxygen consumption rate (OCR), 1 μM oligomycin was added to inhibit ATP synthesis from oxidative phosphorylation. Then 1 μM carbonyl cyanide-4-(trifluoromethoxy)phenylhydrazone (FCCP) was added to uncouple the mitochondrial membrane that stimulates respiration. Lastly, 1 μM rotenone and 1 μM antimycin A (R + A) was added to inhibit complex I and III that terminates mitochondrial oxidative phosphorylation. Basal OCR was calculated as $[OCR_{initial} - OCR_{R+A}]$. Maximum respiration rate was computed as $[OCR_{FCCP} - OCR_{R+A}]$.

Metabolic profiling of acylcarnitines and amino acids

Acylcarnitines and amino acids in BAT were measure in the Duke-NUS Metabolomics Facility according to previously established mass spectrometry (MS)-based methods [64–66]. Briefly, brown adipose tissue was homogenized in 50% acetonitrile and 0.3% formic acid. For acylcarnitine and amino acid extraction, 100 μl of tissue homogenate was extracted using methanol. The acylcarnitine extracts were derivatized with 3 M hydrochloric acid in methanol, dried, and reconstituted in methanol for analysis in liquid chromatography/mass spectrometry (LC/MS). Acylcarnitine measurements were made using flow injection–tandem mass spectrometry on the Agilent 6430 Triple Quadrupole LC/MS system (Agilent Technologies, CA, USA). The sample analysis was carried out at 0.4 ml/min of 80:20 methanol:water as mobile phase and injection of 2 μl of sample. Data acquisition and analysis were performed on Agilent MassHunter Workstation B.06.00 software. Amino acids were separated using a C8 column (Rapid Resolution HT, 4.5 x 50 mm, 1.8 μm, Zorbax SB-C8) on a Agilent 1290 Infinity LC system (Agilent Technologies, CA, USA) coupled with quadrupole-ion trap mass spectrometer (QTRAP 5500, AB Sciex, DC, USA). Mobile phase A (10:90 water:acetonitrile) and Mobile phase B (90:10 water:acetonitrile) both containing 10 mM of ammonium formate were used for chromatography separation. The LC run was performed at a flow rate of 0.6 mL min^{-1} with initial gradient of 20% B for 0.5 min, then ramped to 100% B in 2.5 min, maintained for 0.5 min, followed by re-equilibrating the column to the initial run condition (20% B) for 2 min. All compounds were ionized in positive mode using electrospray ionization. The chromatograms were integrated using MultiQuant™ 3.0 software (AB Sciex, DC, USA).

Electron microscopy

Cells were seeded in a 4-chambered coverglass (Thermo Scientific Nunc, NNU 155383-PK) and allowed to differentiate for 7 d before addition of T_3 or bafilomycin A_1 (Baf; Sigma-Aldrich, B1793). After treatment, cells were fixed with 2.5% glutaraldehyde (nacalai tesque, 17025–25) in sodium phosphate buffer (0.1 M, pH 7.4) and washed 3 times with phosphate buffered saline (PBS; Axil Scientific, BUF-2040-1X1L). The samples were then post-fixed with 1% osmium tetroxide and dehydrated with a series of alcohol with increasing concentration. After embedding samples in Araldite (Pelco, 18060), ultra-thin sections were cut and double-stained with uranyl acetate and lead citrate. Images were taken using the Olympus EM208S transmission electron microscope (Japan).

Statistical analysis

Cell culture experiments were performed in triplicate and independently repeated 3 times. Data were pooled and represented as either mean ± SD for cell culture experiments or mean ± SEM for animal experiments. The statistical significance between sample groups was assessed by the Student t test (2-tailed). One-way ANOVA and the Tukey post-hoc test were performed when comparing different groups.

Acknowledgments

The author would like to thank Dr. Kenji Ohba, Mr. Sherwin Xie, Ms. Andrea Lim, Ms. Sook Yoong Chia, Mr. Ufuk Degirmenci and Dr. Kristmundur Sigmundsson for their helpful advice and technical support. We are thankful to Prof. Jean-Paul Kovalik, Prof. Jianhong Ching, Dr. Cheng Shang See, Kevin Timothy Fridianto, Edison and Kim Huey Ee for performing metabolic profiling (Metabolomics@ Duke-NUS). We would also like to thank Prof. T. Yoshimori (Osaka University, Osaka, Japan) and Dr Andreas Till (Institute of Clinical Molecular Biology Christian-Albrechts-University of Kiel; Kiel, Germany) for gifting plasmids.

Disclosure statement

No potential conflict of interest was reported by the authors.

Funding

The research was funded by NMRC/CIRG/1457/2016 (PMY), NMRC/CSA/0054/2013 (PMY), NMRC/CIRG/1340/2012 (PMY), NMRC/OFYIRG/0002/2016 (BKS) and A*STAR R-913-301-197-304 (SS). This work was supported by the MOH | National Medical Research Council (NMRC) and the Agency for Science, Technology and Research (A*STAR).

References

[1] Bianco AC, Kim BW. Deiodinases: implications of the local control of thyroid hormone action. J Clin Invest. 2006 Oct;116(10):2571–2579. PubMed PMID: 17016550; PubMed Central PMCID: PMCPMC1578599.

[2] Silva JE. The thermogenic effect of thyroid hormone and its clinical implications. Ann Intern Med. 2003 Aug 5;139(3):205–213. PubMed PMID: 12899588.

[3] Bianco AC, Maia AL, da Silva WS, et al. Adaptive activation of thyroid hormone and energy expenditure. Biosci Rep. 2005 Jun-Aug;25(3–4):191–208. PubMed PMID: 16283553.

[4] Obregon MJ. Adipose tissues and thyroid hormones. Front Physiol. 2014;5:479. PubMed PMID: 25566082; PubMed Central PMCID: PMCPMC4263094.

[5] de Jesus LA, Carvalho SD, Ribeiro MO, et al. The type 2 iodothyronine deiodinase is essential for adaptive thermogenesis in brown adipose tissue. J Clin Invest. 2001 Nov;108(9):1379–1385. PubMed PMID: 11696583; PubMed Central PMCID: PMCPMC209445.

[6] Lowell BB, Spiegelman BM. Towards a molecular understanding of adaptive thermogenesis. Nature. 2000 Apr 6;404(6778):652–660. PubMed PMID: 10766252.

[7] Cypess AM, Kahn CR. Brown fat as a therapy for obesity and diabetes. Curr Opin Endocrinol Diabetes Obes. 2010 Apr;17(2):143–149. PubMed PMID: 20160646; PubMed Central PMCID: PMCPMC3593105.

[8] Obregon MJ, Ruiz De Ona C, Hernandez A, et al. Thyroid hormones and 5′-deiodinase in rat brown adipose tissue during fetal life. Am J Physiol. 1989 Nov;257(5 Pt 1):E625–31. PubMed PMID: 2688435.

[9] Hall JA, Ribich S, Christoffolete MA, et al. Absence of thyroid hormone activation during development underlies a permanent defect in adaptive thermogenesis. Endocrinology. 2010 Sep;151(9):4573–4582. PubMed PMID: 20660060; PubMed Central PMCID: PMCPMC2940501.

[10] Christoffolete MA, Linardi CC, de Jesus L, et al. Mice with targeted disruption of the Dio2 gene have cold-induced overexpression of the uncoupling protein 1 gene but fail to increase brown adipose tissue lipogenesis and adaptive thermogenesis. Diabetes. 2004 Mar;53(3):577–584. PubMed PMID: 14988240.

[11] Weiner J, Kranz M, Kloting N, et al. Thyroid hormone status defines brown adipose tissue activity and browning of white adipose tissues in mice. Sci Rep. 2016 Dec;12(6):38124. PubMed PMID: 27941950; PubMed Central PMCID: PMCPMC5150531.

[12] Carvalho SD, Kimura ET, Bianco AC, et al. Central role of brown adipose tissue thyroxine 5′-deiodinase on thyroid hormone-dependent thermogenic response to cold. Endocrinology. 1991 Apr;128(4):2149–2159. PubMed PMID: 2004619.

[13] Bianco AC, McAninch EA. The role of thyroid hormone and brown adipose tissue in energy homoeostasis. Lancet Diabetes Endocrinol. 2013 Nov;1(3):250–258. PubMed PMID: 24622373; PubMed Central PMCID: PMCPMC4976626.

[14] Lopez M, Varela L, Vazquez MJ, et al. Hypothalamic AMPK and fatty acid metabolism mediate thyroid regulation of energy balance. Nat Med. 2010 Sep;16(9):1001–1008. PubMed PMID: 20802499; PubMed Central PMCID: PMCPMC2935934.

[15] Reiter RJ, Klaus S, Ebbinghaus C, et al. Inhibition of 5′-deiodination of thyroxine suppresses the cold-induced increase in brown adipose tissue messenger ribonucleic acid for mitochondrial uncoupling protein without influencing lipoprotein lipase activity. Endocrinology. 1990 May;126(5):2550–2554. PubMed PMID: 2328697.

[16] Cannon B, Nedergaard J. Brown adipose tissue: function and physiological significance. Physiol Rev. 2004 Jan;84(1):277–359. PubMed PMID: 14715917.

[17] Obregon MJ, Pitamber R, Jacobsson A, et al. Euthyroid status is essential for the perinatal increase in thermogenin mRNA in brown adipose tissue of rat pups. Biochem Biophys Res Commun. 1987 Oct 14;148(1):9–14. PubMed PMID: 3118877.

[18] Bianco AC, Sheng XY, Silva JE. Triiodothyronine amplifies norepinephrine stimulation of uncoupling protein gene transcription by a mechanism not requiring protein synthesis. J Biol Chem. 1988 Dec 5;263(34):18168–18175. PubMed PMID: 3192531.

[19] Bianco AC, Kieffer JD, Silva JE. Adenosine 3′,5′-monophosphate and thyroid hormone control of uncoupling protein messenger ribonucleic acid in freshly dispersed brown adipocytes. Endocrinology. 1992 May;130(5):2625–2633. PubMed PMID: 1374009.

[20] Giralt M, Martin I, Iglesias R, et al. Ontogeny and perinatal modulation of gene expression in rat brown adipose tissue. Unaltered iodothyronine 5′-deiodinase activity is necessary for the response to environmental temperature at birth. Eur J Biochem. 1990 Oct 5;193(1):297–302. PubMed PMID: 2171932.

[21] Hernandez A, Obregon MJ. T3 potentiates the adrenergic stimulation of type II 5′-deiodinase activity in cultured rat brown adipocytes. Am J Physiol. 1996 Jul;271(1 Pt 1):E15–23. PubMed PMID: 8760076.

[22] Guerra C, Roncero C, Porras A, et al. Triiodothyronine induces the transcription of the uncoupling protein gene and stabilizes its mRNA in fetal rat brown adipocyte primary cultures. J Biol Chem. 1996 Jan 26;271(4):2076–2081. PubMed PMID: 8567662.

[23] Zhang Y, Goldman S, Baerga R, et al. Adipose-specific deletion of autophagy-related gene 7 (atg7) in mice reveals a role in adipogenesis. Proc Natl Acad Sci USA. 2009 Nov 24;106(47):19860–19865. PubMed PMID: 19910529; PubMed Central PMCID: PMCPMC2785257.

[24] Mottillo EP, Desjardins EM, Crane JD, et al. Lack of adipocyte AMPK exacerbates insulin resistance and hepatic steatosis through brown and beige adipose tissue function. Cell Metab. 2016 Jul 12;24(1):118–129. PubMed PMID: 27411013.

[25] Martinez-Lopez N, Garcia-Macia M, Sahu S, et al. Autophagy in the CNS and periphery coordinate lipophagy and lipolysis in the brown adipose tissue and liver. Cell Metab. 2016 Jan 12;23(1):113–127. PubMed PMID: 26698918; PubMed Central PMCID: PMCPMC4715637.

[26] Sinha RA, Singh BK, Zhou J, et al. Thyroid hormone induction of mitochondrial activity is coupled to mitophagy via ROS-AMPK-ULK1 signaling. Autophagy. 2015;11(8):1341–1357. PubMed PMID: 26103054; PubMed Central PMCID: PMCPMC4590606.

[27] Lesmana R, Sinha RA, Singh BK, et al. Thyroid hormone stimulation of autophagy is essential for mitochondrial biogenesis and activity in skeletal muscle. Endocrinology. 2016 Jan;157(1):23–38. PubMed PMID: 26562261.

[28] Laker RC, Xu P, Ryall KA, et al. A novel MitoTimer reporter gene for mitochondrial content, structure, stress, and damage *in vivo*. J

Biol Chem. 2014 Apr 25;289(17):12005–12015. PubMed PMID: 24644293; PubMed Central PMCID: PMCPMC4002107.
[29] Hernandez G, Thornton C, Stotland A, et al. MitoTimer: a novel tool for monitoring mitochondrial turnover. Autophagy. 2013 Nov 1;9(11):1852–1861. PubMed PMID: 24128932; PubMed Central PMCID: PMCPMC4028337.
[30] Lynch CJ. Role of leucine in the regulation of mTOR by amino acids: revelations from structure-activity studies. J Nutr. 2001 Mar;131(3):861S–865S. PubMed PMID: 11238775.
[31] Jewell JL, Russell RC, Guan KL. Amino acid signalling upstream of mTOR. Nat Rev Mol Cell Biol. 2013 Mar;14(3):133–139. PubMed PMID: 23361334; PubMed Central PMCID: PMCPMC3988467.
[32] Bar-Peled L, Sabatini DM. Regulation of mTORC1 by amino acids. Trends Cell Biol. 2014 Jul;24(7):400–406. PubMed PMID: 24698685; PubMed Central PMCID: PMCPMC4074565.
[33] Boutant M, Joffraud M, Kulkarni SS, et al. SIRT1 enhances glucose tolerance by potentiating brown adipose tissue function. Mol Metab. 2015 Feb;4(2):118–131. PubMed PMID: 25685699; PubMed Central PMCID: PMCPMC4314542.
[34] Ghosh HS, McBurney M, Robbins PD. SIRT1 negatively regulates the mammalian target of rapamycin. PLoS One. 2010 Feb 15;5(2):e9199. PubMed PMID: 20169165; PubMed Central PMCID: PMCPMC2821410.
[35] Broeders EP, Vijgen GH, Havekes B, et al. Thyroid hormone activates brown adipose tissue and increases non-shivering thermogenesis–a cohort study in a group of thyroid carcinoma patients. PLoS One. 2016;11(1):e0145049. PubMed PMID: 26784028; PubMed Central PMCID: PMCPMC4718641.
[36] Lahesmaa M, Orava J, Schalin-Jantti C, et al. Hyperthyroidism increases brown fat metabolism in humans. J Clin Endocrinol Metab. 2014 Jan;99(1):E28–35. PubMed PMID: 24152690.
[37] Silva JE, Larsen PR. Hormonal regulation of iodothyronine 5′-deiodinase in rat brown adipose tissue. Am J Physiol. 1986 Dec;251(6 Pt 1):E639–43. PubMed PMID: 3538896.
[38] Zhang Y, Zeng X, Jin S. Autophagy in adipose tissue biology. Pharmacol Res. 2012 Dec;66(6):505–512. PubMed PMID: 23017672.
[39] Lin JZ, Martagon AJ, Cimini SL, et al. Pharmacological activation of thyroid hormone receptors elicits a functional conversion of white to brown fat. Cell Rep. 2015 Nov 24;13(8):1528–1537. PubMed PMID: 26586443; PubMed Central PMCID: PMCPMC4662916.
[40] Altshuler-Keylin S, Shinoda K, Hasegawa Y, et al. Beige adipocyte maintenance is regulated by autophagy-induced mitochondrial clearance. Cell Metab. 2016 Sep 13;24(3):402–419. PubMed PMID: 27568548; PubMed Central PMCID: PMCPMC5023491.
[41] Armani A, Cinti F, Marzolla V, et al. Mineralocorticoid receptor antagonism induces browning of white adipose tissue through impairment of autophagy and prevents adipocyte dysfunction in high-fat-diet-fed mice. FASEB J. 2014 Aug;28(8):3745–3757. PubMed PMID: 24806198.
[42] Cannon B, Nedergaard J. Thyroid hormones: igniting brown fat via the brain. Nat Med. 2010 Sep;16(9):965–967. PubMed PMID: 20823876.
[43] Harms M, Seale P. Brown and beige fat: development, function and therapeutic potential. Nat Med. 2013 Oct;19(10):1252–1263. PubMed PMID: 24100998.
[44] Martinez-Lopez N, Athonvarangkul D, Sahu S, et al. Autophagy in Myf5+ progenitors regulates energy and glucose homeostasis through control of brown fat and skeletal muscle development. EMBO Rep. 2013 Sep;14(9):795–803. PubMed PMID: 23907538; PubMed Central PMCID: PMCPMC3790054.
[45] Lopez-Soriano FJ, Alemany M. Activities of enzymes of amino acid metabolism in rat brown adipose tissue. Biochem Int. 1986 Mar;12(3):471–478. PubMed PMID: 2871838.
[46] Lopez-Soriano FJ, Fernandez-Lopez JA, Mampel T, et al. Amino acid and glucose uptake by rat brown adipose tissue. Effect of cold-exposure and acclimation. Biochem J. 1988 Jun 15;252 (3):843–849. PubMed PMID: 3421924; PubMed Central PMCID: PMCPMC1149224.
[47] Hatazawa Y, Tadaishi M, Nagaike Y, et al. PGC-1alpha-mediated branched-chain amino acid metabolism in the skeletal muscle. PLoS One. 2014;9(3):e91006. PubMed PMID: 24638054; PubMed Central PMCID: PMCPMC3956461.
[48] Demine S, Tejerina S, Bihin B, et al. Mild mitochondrial uncoupling induces HSL/ATGL-independent lipolysis relying on a form of autophagy in 3T3-L1 adipocytes. J Cell Physiol. 2018 Feb;233 (2):1247–1265. PubMed PMID: 28488768.
[49] Goglia F, Moreno M, Lanni A. Action of thyroid hormones at the cellular level: the mitochondrial target. FEBS Lett. 1999 Jun 11;452 (3):115–120. PubMed PMID: 10386574.
[50] Singh BK, Sinha RA, Zhou J, et al. Hepatic FOXO1 target genes are co-regulated by thyroid hormone via RICTOR protein deacetylation and MTORC2-AKT protein inhibition. J Biol Chem. 2016 Jan 1;291(1):198–214. PubMed PMID: 26453307; PubMed Central PMCID: PMCPMC4697156.
[51] Gerhart-Hines Z, Dominy JE Jr., Blattler SM, et al. The cAMP/PKA pathway rapidly activates SIRT1 to promote fatty acid oxidation independently of changes in NAD(+). Mol Cell. 2011 Dec 23;44(6):851–863. PubMed PMID: 22195961; PubMed Central PMCID: PMCPMC3331675.
[52] Cairo M, Villarroya J, Cereijo R, et al. Thermogenic activation represses autophagy in brown adipose tissue. Int J Obes (Lond). 2016 Jun 24;40:1591–1599. PubMed PMID: 27339605.
[53] Gao M, Zhang C, Ma Y, et al. Cold exposure improves the anti-diabetic effect of T0901317 in streptozotocin-induced diabetic mice. AAPS J. 2015 May;17(3):700–710. PubMed PMID: 25739819; PubMed Central PMCID: PMCPMC4406970.
[54] Watanabe M, Yamamoto T, Kakuhata R, et al. Synchronized changes in transcript levels of genes activating cold exposure-induced thermogenesis in brown adipose tissue of experimental animals. Biochim Biophys Acta. 2008 Jan;1777(1):104–112. PubMed PMID: 18036333.
[55] Sanchez-Alavez M, Conti B, Wood MR, et al. ROS and sympathetically mediated mitochondria activation in brown adipose tissue contribute to methamphetamine-induced hyperthermia. Front Endocrinol (Lausanne). 2013;4:44. PubMed PMID: 23630518; PubMed Central PMCID: PMCPMC3632801.
[56] Barja de Quiroga G, Lopez-Torres M, Perez-Campo R, et al. Effect of cold acclimation on GSH, antioxidant enzymes and lipid peroxidation in brown adipose tissue. Biochem J. 1991 Jul 1;277(Pt 1):289–292. PubMed PMID: 1854342; PubMed Central PMCID: PMCPMC1151223.
[57] Petrovic V, Buzadzic B, Korac A, et al. Antioxidative defense and mitochondrial thermogenic response in brown adipose tissue. Genes Nutr. 2010 Sep;5(3):225–235. PubMed PMID: 20012899; PubMed Central PMCID: PMCPMC2935534.
[58] Cypess AM, Weiner LS, Roberts-Toler C, et al. Activation of human brown adipose tissue by a beta3-adrenergic receptor agonist. Cell Metab. 2015 Jan 6;21(1):33–38. PubMed PMID: 25565203; PubMed Central PMCID: PMCPMC4298351.
[59] Mizushima N, Yamamoto A, Matsui M, et al. *In vivo* analysis of autophagy in response to nutrient starvation using transgenic mice expressing a fluorescent autophagosome marker. Mol Biol Cell. 2004 Mar;15(3):1101–1111. PubMed PMID: 14699058; PubMed Central PMCID: PMCPMC363084.
[60] Hara T, Nakamura K, Matsui M, et al. Suppression of basal autophagy in neural cells causes neurodegenerative disease in mice. Nature. 2006 Jun 15;441(7095):885–889. PubMed PMID: 16625204.
[61] Rehnmark S, Kopecky J, Jacobsson A, et al. Brown adipocytes differentiated in vitro can express the gene for the uncoupling protein thermogenin: effects of hypothyroidism and norepinephrine. Exp Cell Res. 1989 May;182(1):75–83. PubMed PMID: 2497023.
[62] Klein J, Fasshauer M, Ito M, et al. beta(3)-adrenergic stimulation differentially inhibits insulin signaling and decreases insulin-induced glucose uptake in brown adipocytes. J Biol Chem. 1999 Dec 3;274(49):34795–34802. PubMed PMID: 10574950.

[63] Wu Y, Smas CM. Expression and regulation of transcript for the novel transmembrane protein Tmem182 in the adipocyte and muscle lineage. BMC Res Notes. 2008 Sep 19;1:85. PubMed PMID: 18803820; PubMed Central PMCID: PMCPMC2564950.

[64] Muoio DM, Noland RC, Kovalik JP, et al. Muscle-specific deletion of carnitine acetyltransferase compromises glucose tolerance and metabolic flexibility. Cell Metab. 2012 May 2;15(5):764–777. PubMed PMID: 22560225; PubMed Central PMCID: PMCPMC3348515.

[65] Newgard CB, An J, Bain JR, et al. A branched-chain amino acid-related metabolic signature that differentiates obese and lean humans and contributes to insulin resistance. Cell Metab. 2009 Apr;9(4):311–326. PubMed PMID: 19356713; PubMed Central PMCID: PMCPMC3640280.

[66] Sinha RA, Farah BL, Singh BK, et al. Caffeine stimulates hepatic lipid metabolism by the autophagy-lysosomal pathway in mice. Hepatology. 2014 Apr;59(4):1366–1380. PubMed PMID: 23929677.